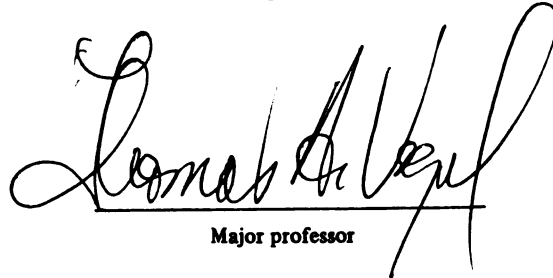THESIS
2

This is to certify that the

thesis entitled

Petrogenesis of the Keetley Volcanics in
Summit and Wasatch Counties, North-Central
Utah
presented by

LeeAnn Feher

has been accepted towards fulfillment
of the requirements for

___M.S.___ degree in _Geology_

_____
Major professor

Date_4-7-97_____

PLACE IN RETURN BOX to remove this checkout from your record.
TO AVOID FINES return on or before date due.

DATE DUE	DATE DUE	DATE DUE
_____	_____	_____
_____	_____	_____
_____	_____	_____
_____	_____	_____
_____	_____	_____
_____	_____	_____
_____	_____	_____

MSU Is An Affirmative Action/Equal Opportunity Institution

c:\circ\datedue.pm3-p.1

PETROGENENIS OF THE KEETLEY VOLCANICS, IN SUMMIT AND WASATCH COUNTIES, NORTH-CENTRAL UTAH

by

LeeAnn Feher

A THESIS

Submitted to

Michigan State University

in partial fulfillment of the requirements

for the degree of

MASTER OF SCIENCE

Department of Geological Sciences

1997

ABSTRACT

PETROGENESIS OF THE KEETELY VOLCANICS, IN SUMMIT AND WASATCH COUNTIES, NORTH-CENTRAL UTAH

by

LeeAnn Feher

The Oligocene Keetley volcanics (KV) are located in north-central Utah and occur on the eastern end of the 45-kilometer long, east-west trending, Wasatch intrusive belt (WIB). The WIB is part of the Cottonwood Arch and occurs along the extension of the Uinta Arch.

The KV and the Wasatch intrusive rocks are a series of high-K, calc-alkaline rocks. The WIB consists of a western group and an eastern group of stocks. The western stocks consist of three chemically distinct stocks; the Little Cottonwood, Alta and Clayton Peak, the eastern stocks are chemically similar to the Alta stock. The KV are similar to the eastern stocks and the Alta stock with respect to emplacement ages and chemical composition. The chemical composition of the KV ranges from 55 wt. % SiO_2 to 68 wt. % SiO_2 and there is little variation in mineralogy. In comparison with other well-documented calc-alkaline rocks the KV do not follow typical, coherent calc-alkaline chemical trends nor do they follow simple crystal fractionation and/or assimilation paths, thus the origin of the chemical variation is most likely due to complex processes involving multiple magmatic sources. The origin of the WIB and KV is probably related to partial melting of the crust due to production of decompression mantle melts resulting from the rollback of the Farallon plate which occurred in the Cordillera beginning 50 Ma.

For T and Mick.

ACKNOWLEDGEMENTS

Thanks Mom and Dad. I couldn't have done this without your support. Lisa, my sister, thank you for all the laughs when I needed them and all the cat care-taking that allowed me to go on my adventures. Special thanks to Candice Murphy, my very best friend in the whole world.

I thank Tom Vogel, my advisor, and Kathy Fishburn for all their support since my arrival at MSU. Thanks Tom for being an excellent role model and for all your guidance, especially in my moments of foundering. Bill Cambray and Kaz Fugita, my committee members are thanked for their input and reviews of this thesis.

I would also like to thank my original inspirations, Tim Flood and Nelson Ham who got me started on all this geology in the first place.

TABLE OF CONTENTS

LIST OF TABLES

LIST OF FIGURES

INTRODUCTION

The Oligocene Keetley volcanics are located in north-central Utah and occur on the eastern end of the 45-kilometer long, east-west trending, Wasatch intrusive belt (Figure 1) (John, 1989). The Wasatch intrusive belt is part of the Cottonwood Arch and is continuous with the western extension of the Uinta Arch. The Keetley volcanics and the Wasatch intrusive rocks are a series of high-K, calc-alkaline rocks. These are divided into two groups of stocks and a sequence of volcanic rocks based on the relative location and differences in texture among the stocks. The western stocks are coarse-grained, mostly equigranular and include the Little Cottonwood, Alta, and Clayton Peak stocks. The eastern stocks are in general porphyritic, characterized by coarse-grained phenocrysts in a fine- to medium-grained groundmass, and include the Flagstaff, Ontario, Mayflower, Glencoe, Valeo, Pine Creek, and Park Premier stocks and the Indian Hollow plug. The two latter stocks occur in the very eastern end of the area and intrude the Keetley volcanics (Figure 2) (John, 1989). The Indian Hollow plug is not shown on Figure 2 but occurs just to the north-east of the Park Premier stock. The Keetley volcanics are a high-K andesitic sequence of lahars, volcanic conglomerates, tuffs and breccias, and minor lava flows (Leveinen, 1984). The clasts within the Keetley volcanics are characterized by fine- to medium-grained phenocrysts in a mostly fine-grained matrix. The Keetley volcanics have an estimated maximum thickness of at least 90 m near the Jordanelle Dam just east of Park City, Utah (Woodfill, 1972) and extend over 330 km^2 of area in north-central Utah. The Keetley volcanics have been deposited subhorizontally between the west-east trending Uinta Arch to the east and the north-south trending Wasatch Range to the west.

1
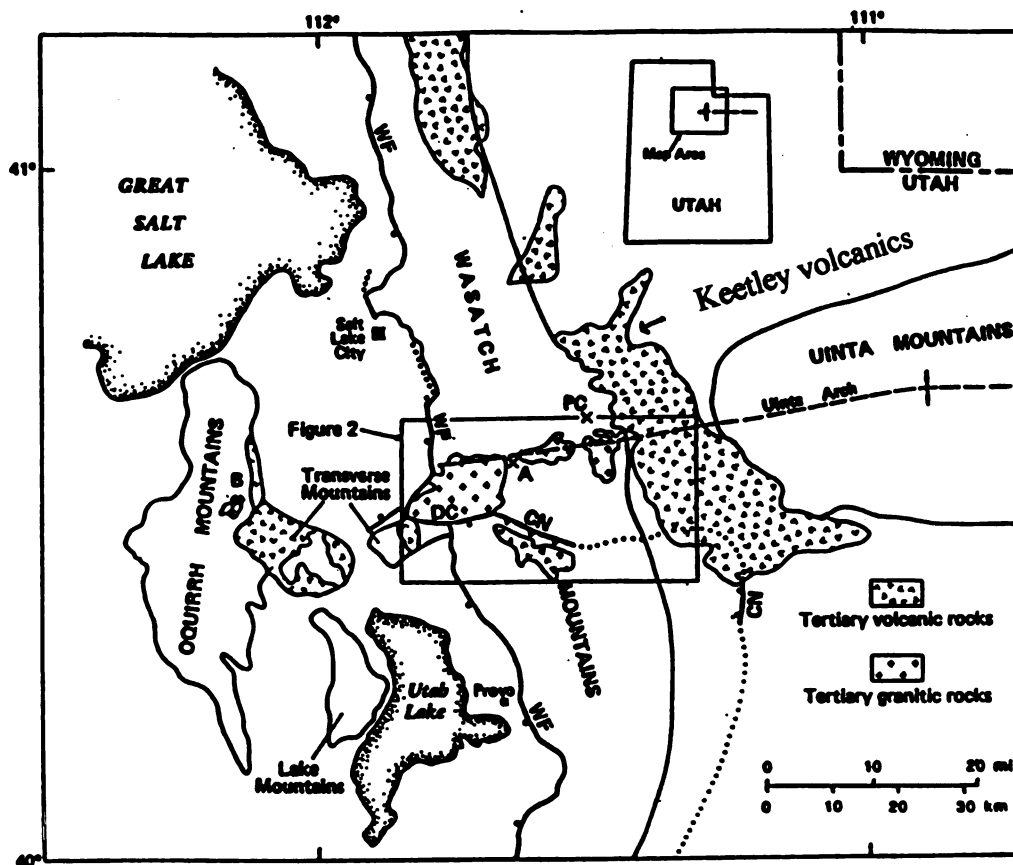
Figure 1.   Location of the Wasatch intrusive belt and the Keetley volcanics in north-central Utah. Boxed area is the map area from John's map (1989). The Keetley volcanics are the southern most group of Tertiary volcanics. Modified from John (1989). PC = Pine Creek, A = Alta, WF = Wasatch Front, CN = Charleston-Nebo, DC = Deer Creek.

3
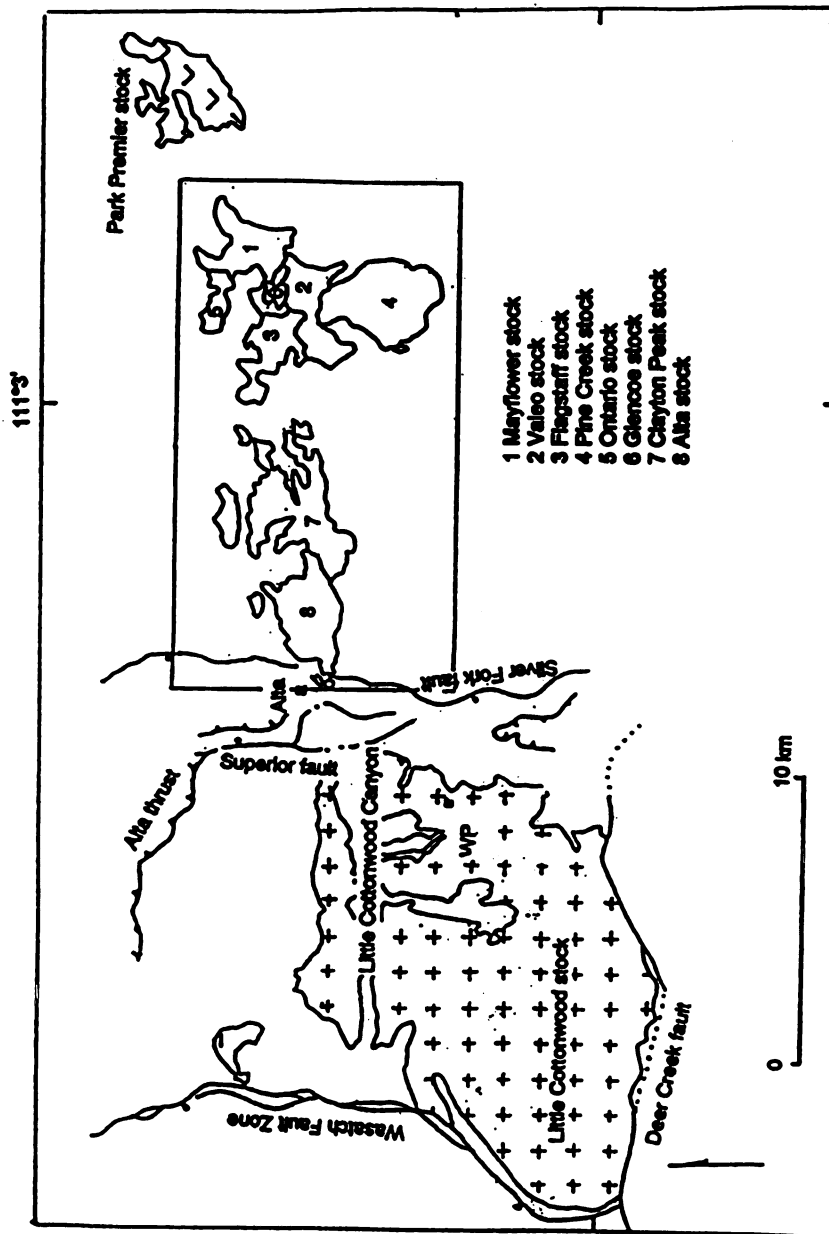
Figure 2.　Close up of the Wasatch intrusive belt, illustrating the nine stocks as well as the Park Premier stock, the Indian Hollow plug is off the map area just to the northeast of the Park Premier stock. The Park Premier stock and the Indian Hollow plug intrude the Keetley volcanics. Modified from John (1989). The area in the smaller rectangle outlines the 8 stocks numbered from 1 through 8.

4

Previous Work

John (1989) estimated the depths of emplacement of the Wasatch intrusive belt based on fluid inclusion data and contact metamorphic mineral assemblages as well as stratigraphic relationships. The estimated depths of emplacement progressively shallow from west to east with an estimated depth of the Little Cottonwood stock at 11 km in the west and of the eastern stocks at 1 km in the east (John, 1989) (Figure 3). The Keetley volcanics are the eastern most extrusive component of this whole system.

Previously determined ages have shown that the stocks of the Wasatch intrusive belt all have approximately the same age ranging from 30 to 34 Ma (Bromfield, 1977) and (Crittenden, 1973). Detailed U/Pb dating of zircons (Constenius, pers. comm., 1996), and $^{40}Ar/^{39}Ar$ dating (Flood, pers. comm., 1996) of minerals are in progress and may give more insight into the age relationships within the Wasatch intrusive belt.

Based on research in progress (Vogel, pers. comm., 1996) three distinct chemical trends occur in the three western stocks (Little Cottonwood, Alta, and Clayton Peak). The eastern stocks, in a gross sense, are chemically similar to the Alta stock. A goal of this study is to compare the chemical compositions of the Keetley volcanics and the Wasatch intrusive belt. Woodfill (1972) presented chemical analyses on seven samples from the Keetley volcanic field. From his work he concluded that the Keetley volcanics were derived from a trachyandesite parent. This model will be evaluated in this study.

5
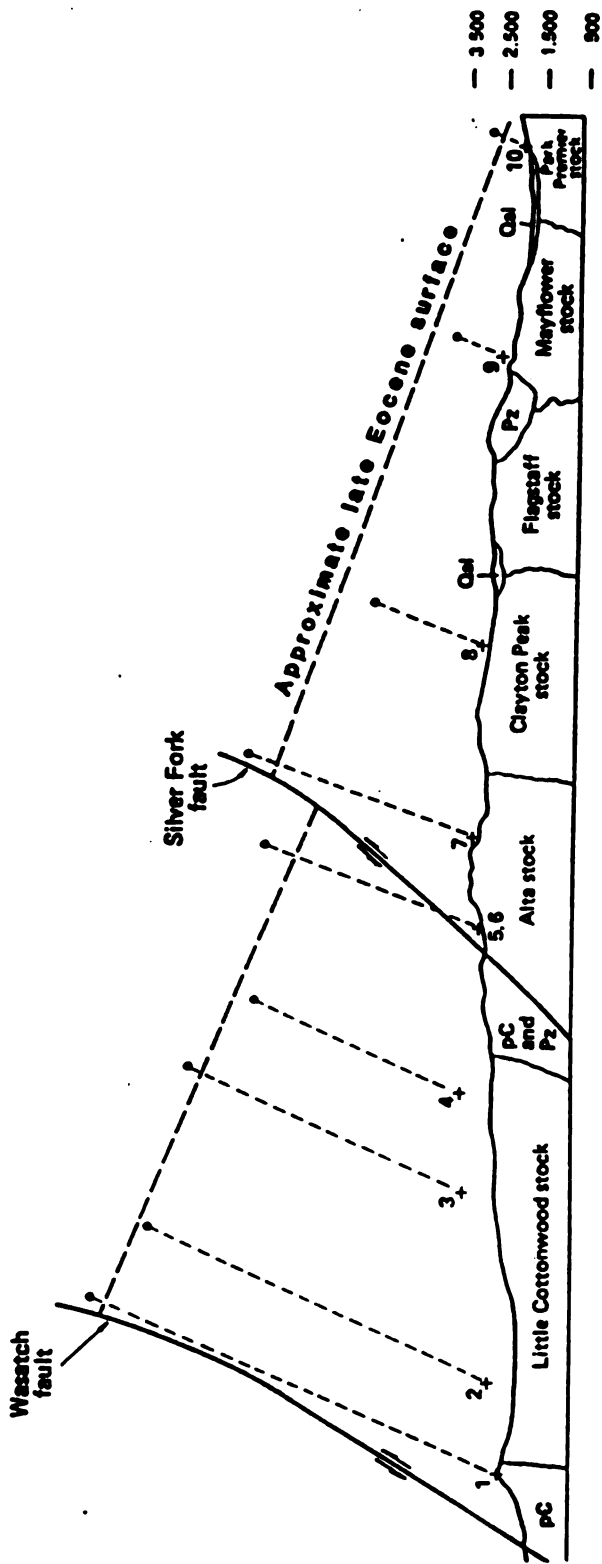
Figure 3.   Schematic cross-section illustrating locations where estimated depths of
             emplacement were made from west to east along the Wasatch intrusive
             belt. The Little Cottonwood was emplaced at 11 km and the eastern most
             stocks were emplaced at about 1 km. From John (1989).

Purpose

The purpose of this study is two-fold. Relationships between the Wasatch intrusive belt and the Keetley volcanics will be determined by comparing chemical compositions and ages. The second part of this thesis is to determine if the origin of the compositional diversity of the Keetley volcanics was produced by differentiation of a single or multiple magmatic sources. In order to do this, the chemical and mineralogical variations will be determined and fractional crystallization, mixing, and assimilation models will be evaluated.

Regional Geology

The Wasatch intrusive belt is located in the central Wasatch Mountains and is considered to be part of the Cottonwood area (Crittenden, 1977). The Wasatch Range extends from the center of Utah, northward into Idaho. The western edge of the range marks part of the eastern limit of the Basin and Range province and the eastern edge, which in many places is not well defined, merges with the Wyoming Basin and the southern Colorado Plateau. The east-west trending Uinta Range separates the Wyoming Basin to the north and the Colorado Plateau to the south. All of these structures are part of the Cordilleran fold and thrust belt (Crittenden, 1977). The Wasatch intrusive belt also lies at the boundary between Archean basement to the north and Proterozoic basement to the south (Hutchinson and Albers, 1992). The junction between Archean and Proterozoic crust forms a weakness at the Uinta trend which extends west of Colorado through the Wasatch Mountains to central Nevada (Bryant and Nichols, 1988).

The Cottonwood area lies at the boundary of the intersection of the Sevier orogenic belt and the east-west trending Uinta arch. Sedimentary units ranging from Precambrian through Mesozoic cratonal and miogeoclinal sediments are intruded by the nine Tertiary plutons of the Wasatch intrusive belt and as a result the sedimentary rocks now dip away from the west-east trend of the intrusive belt to the north, northwest, northeast, east and southeast, most notably near the Little Cottonwood stock and less obviously around the other stocks (Boutwell, 1912). The Keetley volcanics lie subhorizontally between the west-east trending axis of the Uinta Arch and the north-south trending Wasatch Mountains where they cover any structural continuities that may exist between the two major structures (Boutwell, 1912).

By Late Cretaceous time the convergent continental margin of western U.S. had developed into an Andean type continental margin arc system due to subduction of the Farallon plate under the North American plate (Miller et al., 1992, and references therein). During the Late Cretaceous through early Tertiary time, the Laramide and Sevier orogenic events caused by the convergence of the Farallon plate and the North American plate formed the Cordilleran foreland fold and thrust belt in Utah, Idaho and Nevada. The Laramide orogeny took place from 80 to 50 Ma (Miller, 1992) and the Sevier orogeny took place between 145 to 75 Ma (Armstrong, 1968). The eastern extent of the Sevier orogeny is referred to as the hingeline. The deformation caused by the Laramide style deformation occurred mainly within the Colorado Plateau to the east of the hingeline. Predominately thick-skinned deformational foreland uplifts and basins were produced in an area with relatively thin sedimentary cover on Precambrian crystalline basement. The Sevier orogenic event occurred to the west of the hingeline and produced thin-skinned,

decollement thrusting with folding being restricted to the thick miogeoclinal sedimentary wedge and bordering cratonal strata that overlie the Precambrian basement (Miller, 1992). More than half of the total shortening that occurred during the Sevier orogeny happened simultaneously with the basement cored uplifts of the Laramide orogeny (Allmendinger, 1992). Hence, the two styles of deformation were occurring simultaneously for a time.

The Keetley volcanics are bounded by the eastward plunging Cottonwood Arch and the westward plunging Uinta Arch. The Uinta Arch consists of Precambrian through Mesozoic strata that forms a westward plunging anticline. The Uinta Arch was uplifted during the Sevier orogeny and as a result is faulted on both flanks of the main anticline (Crittenden, 1977). Thrust faults developed in the Cottonwood Arch during the Laramide orogenic event. Prior to intrusion of the igneous rocks, large thrust faults and folds formed due to west to east ramping of thick sequences of sedimentary rocks. These faults have a present eastward dip but at the time of formation had a westward dip (Calkins, 1943). It is thought that the present eastward dip of these thrust faults was caused by continued compression from the west that was resisted by the Uinta Arch (Eardley, 1939).

The Cordilleran foreland fold and thrust belt has undergone a number of episodes of extension, but the most notable extension occurred in the Cenozoic. The Cenozoic extensional event formed what is known as the Basin and Range province. Extension occurred mainly in those areas that underwent shortening during the Mesozoic and early Cretaceous times. The general direction of extension was originally east-west and eventually rotated to northwest-southeast. The extension was accommodated by high-angle normal faulting and detachment faults (Wernicke, 1992). Constenius (1996) has

recently illustrated that the Cordilleran foreland fold and thrust belt was reactivated due to a gravitational collapse caused by changes in the rate and style of North America-Pacific plate convergence. A change from compression to extension began with the westward rollback of the Farallon plate beginning at ca. 49-48 Ma and ending ca. 20 Ma (Constenius, 1996). One local effect of the change from compression to extension noted by Constenius (1996) is illustrated by the collapse of the Charleston-Nebo thrust sheet that has been reactivated since compression and has moved westward.

The overall importance of the chemical and age relationships of the Keetley volcanics and the Wasatch intrusive belt to the regional geology is how the timing of emplacement of the magmas relates to the timing of the change from compression to extension in the Cordillera

Methods

Because the Keetley volcanics consist mainly of volcaniclastics, no stratigraphic correlation within a field site or between field sites could be made. Therefore, the sampling strategy that was undertaken was to collect as wide of a variety of volcanic clasts as possible in order to sample the entire chemical variation within the volcanic sequence. Approximately 200 samples were collected from five different locations within the Keetley volcanic field. A total of 50 representative samples were chosen for analyses and added to 17 previously analyzed samples to give a total of 67 chemical analyses.

Several laboratory methods were used to obtain the necessary chemical and mineralogical data for this study. Petrographic analysis of thin sections was done to determine the mineralogy and textures. X-ray fluorescence spectrometry was used to

determine whole rock major element and select trace element concentrations on 67

samples. Electron microprobe analysis was done at the University of Indiana using a

Cameca Camabax SX50 electron microprobe to determine specific major element

chemical compositions of phenocrysts and some microphenocrysts in selected samples.

Statistical multiple linear regression to test fractional crystallization, mixing and

assimilation models were used to evaluate possible petrologic processes as explanations

for the chemical variation within the Keetley volcanics.

X-ray fluorescence techniques involved measuring 1.0 g of finely ground rock

powder, 9.0 g of Lithium Tetraborate and .160 g of Ammonium Nitrate. These materials

were then mixed and fused into glass disks by melting in platinum crucibles for at least 20

minutes and subsequently poured into platinum molds and quenched. Each sample was

then analyzed for major and trace elements using a X-ray fluorescence spectrometer. The

detection limits and standard deviations for the trace elements as well as the trimmed mean

and standard deviations based on 16 repetitions for each major element are reported in

Appendix A.

Electron Microprobe analytical techniques involved obtaining two to three

analyses from each of the selected phenocryst grains including plagioclase, hornblende,

pyroxene and biotite. Ten thin sections were chosen with 8 to 10 phenocrysts selected

from each for analysis. The thin sections were chosen to represent an array of the most

mafic, intermediate and most silicic end members out of the total sample array. In general,

rim compositions were obtained for all selected phenocrysts and in some cases, such as for

reversed zoned plagioclase, rim, middle, and core compositions were obtained. The probe

conditions varied depending on the mineral being analyzed. For mafic silicates a 15 kv

accelerating voltage and a 20 nA beam was used. The beam size was 2 microns. For feldspars a 15 kv accelerating voltage and a 10 to 15 nA beam were used with a beam size of 5 microns.

Wasatch Intrusive Belt Whole Rock Chemical Compositions, Mineralogy and Ages

Major and trace element chemical compositions

The Wasatch intrusive belt consists of nine stocks. These stocks are divided into three western stocks, the Little Cottonwood, Alta, and Clayton peak; and six eastern stocks, the Mayflower, Valeo, Flagstaff, Pine Creek, Ontario and Glencoe. All chemical data for the western and eastern stocks are from Vogel (pers. comm., 1996) The western stocks make up three distinct chemical groups based on major and trace element variation diagrams. The Little Cottonwood stock is the most silicic at about 70% SiO_2, the Alta is intermediate at 60 - 67% SiO_2 and the Clayton Peak is the most mafic at 55% - 60% SiO_2. Rb/Sr - oxide trends as well as major and trace element variation diagrams illustrate the three distinct chemical groups of the western stocks (Figure 4). The eastern stocks are not as chemically diverse as the western stocks. They range in SiO_2 from about 58% to 68% and can not be isolated from each other in terms of distinct chemical groups (Figure 5). In terms of Rb/Sr - oxide trends and major and trace element variation diagrams, it is difficult to separate the eastern stocks from one another with the exception of the Ontario stock which has the highest Rb/Sr content (Figure 5). In a broad comparison, the eastern stocks are most similar to the Alta stock.
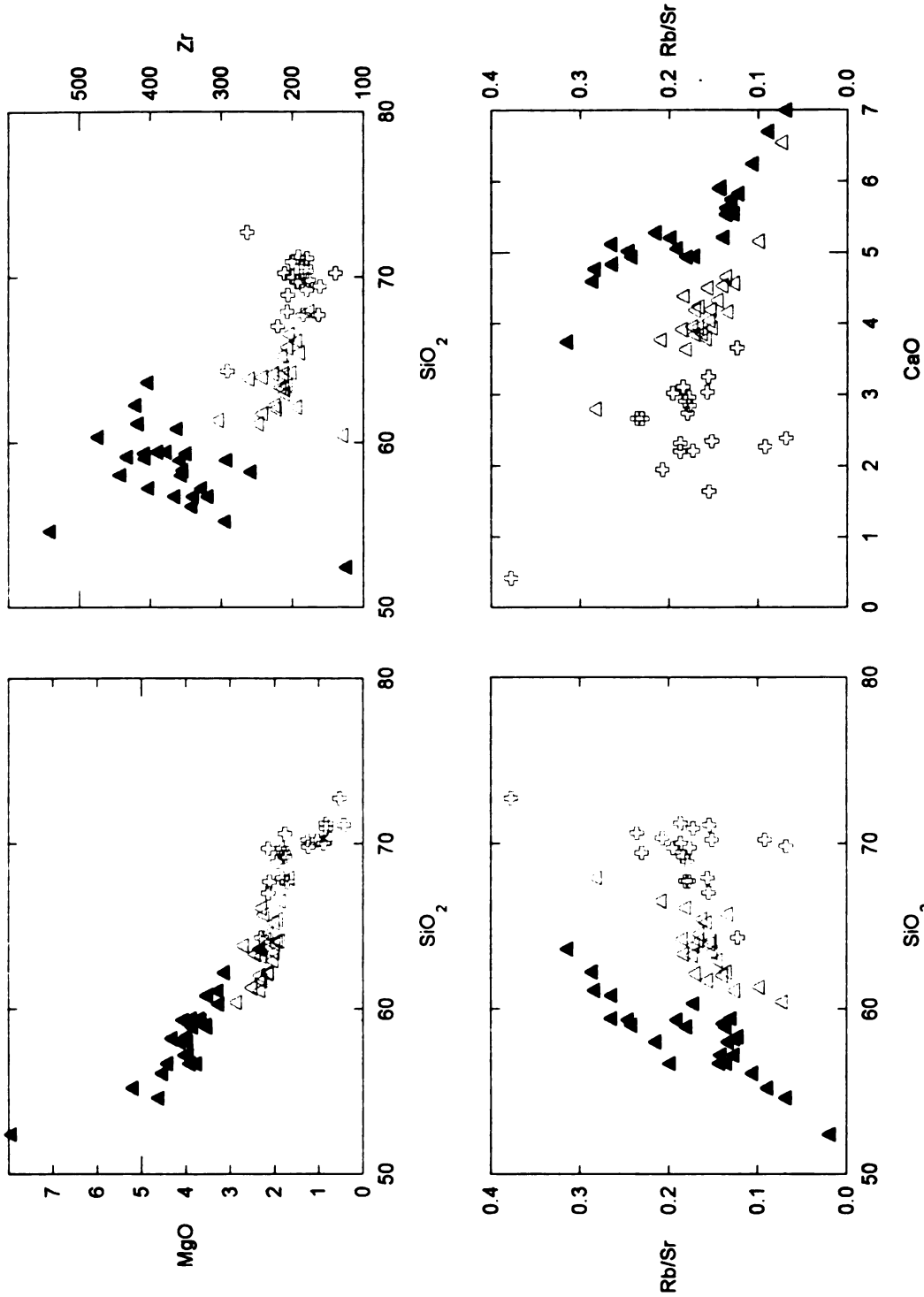
Figure 4. Some major and trace element chemical compositions for the Western stocks. Open crosses are the Little Cottonwood, open triangles are the Alta and filled triangles are the Clayton Peak.

13
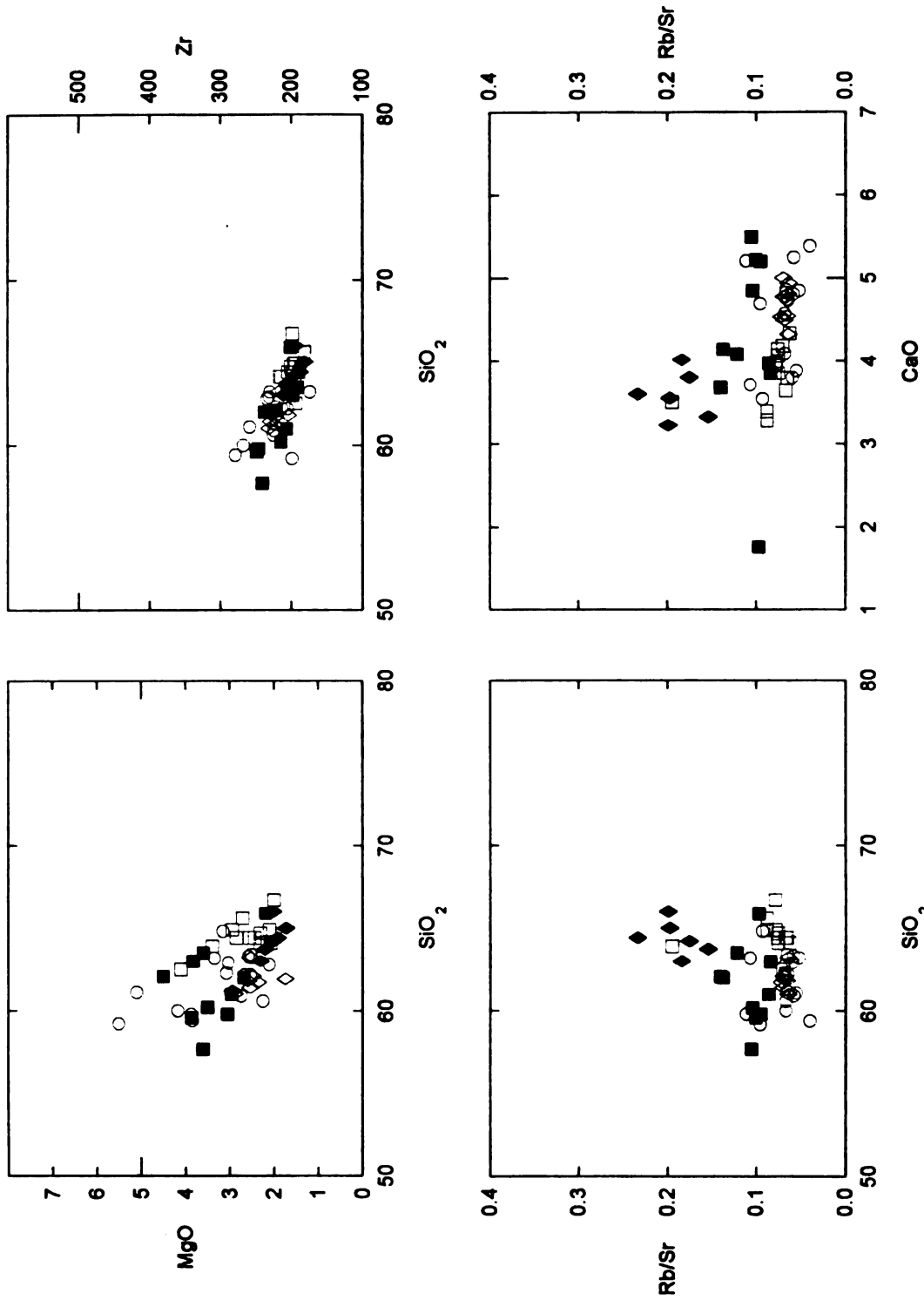
Figure 5. Some major and trace element chemical compositions of the Eastern Stocks. Open circles are for Flagstaff, open squares are for Valeo, filled squares are for Mayflower, open diamonds are for the Pine Creek and filled diamonds are for Ontario.

Summary of the Mineralogy and Textures of the Wasatch Intrusive Belt

John (1989) summarizes the textures and mineralogy of the Wasatch intrusive belt. In general the western stocks range from medium- to coarse-grained for the Little Cottonwood to medium-grained for the Alta and fine-grained for the Clayton Peak. Parts of the Little Cottonwood and the Alta are porphyritic. The eastern stocks range from medium- to fine-grained with seriate porphyritic textures and groundmass ranging in size from .01 - .25 mm overall (John, 1989). The Keetley volcanics are characteristically porphyritic with fine to medium-grained phenocrysts.

In terms of mineralogy, the Little Cottonwood contains K-feldspar phenocrysts up to 6 cm, quartz and biotite, magnetite and sphene with minor hornblende. The Alta stock contains phenocrysts of K-feldspar, plagioclase, quartz and biotite, hornblende, magnetite, sphene and minor amounts of clinopyroxene and illmenite. The Clayton Peak stock has phenocrysts of K-feldspar from 1-2 cm, quartz and rare phenocrysts of biotite and contains clinopyroxene, biotite, magnetite and minor amounts of orthopyroxene, illmenite, sphene and hornblende. The eastern stocks contain plagioclase, biotite, hornblende, magnetite and quartz. The Park Premier also contains clinopyroxene, but no quartz. Some of the eastern stocks contain sphene. The Keetley volcanics contain plagioclase, hornblende, clinopyroxene, rare orthopyroxene, biotite and rare sphene as well as resorbed quartz.

Ages

Ages for the Wasatch intrusive belt including the Keetley volcanics are listed in Table 1. Biotite K/Ar ages (closing temperature 310°) of the Wasatch intrusive belt and Keetley volcanics were determined by Bromfield and others (1977) and Crittenden and

Table 1. Ages for the Wasatch intrusive belt and the Keetley volcanics.

Western stocks

Igneous Body	Age	Method	Source
Little Cottonwood	25.1	K/Ar Biot	C
	27.3	K/Ar Biot	C
	25.5	K/Ar Musc	C
	31.1	K/Ar Hbl	C
	30.2	U/Pb	K.C.
	30.5	U/Pb	K.C.
Alta	31.6	K/Ar Biot	B
	31.7	K/Ar Biot	B
	32.1	K/Ar Biot	B
	32.1	K/Ar Biot	C
	32.6	K/Ar Biot	C
	32.8	K/Ar Biot	C
	32.4	K/Ar Biot	C
	46.6	K/Ar Hbl	B
	46.7	K/Ar Hbl	B
	33.5	K/Ar Hbl	C
	30.9	K/Ar Hbl	C
	35.1	K/Ar Hbl	C
	33.5	U/Pb	K.C.
	35.0	U/Pb	K.C.
Clayton Peak	32.9	K/Ar Biot	B
	34.8	K/Ar Biot	B
	36.7	K/Ar Biot	C

Eastern Stocks

Igneous Body	Age	Method	Source
Pine Creek		35.2 K/Ar Biot	B
		36.8 K/Ar Biot	C
Valeo		40.3 K/Ar Biot	B
		39.8 K/Ar Biot	B
Flagstaff		39.7 K/Ar Hbl	B
		37.8 K/Ar Hbl	B
Mayflower		41.2 K/Ar Hbl	B
Ontario		35.6 U/Pb	K.C.
		35.7 U/Pb	K.C.
		33.4 K/Ar Biot	B
		34.0 K/Ar Biot	B
		33.7 K/Ar Biot	B
		34.5 K/Ar Biot	B
		33.3 K/Ar Biot	B
Park Premier		33.9 K/Ar Biot	B
		35.2 K/Ar Hbl	B
Indian Hollow		36.2 K/Ar Biot	K/Ar Hbl
Keetley volcanics		35.1 K/Ar Biot	C
		32.7 K/Ar Biot	C
		34 K/Ar Biot	C
		33.9 K/Ar Hbl	K/Ar Hbl
		36.4 K/Ar Hbl	K/Ar Hbl

K.C. = Constenius (1996)
B = Bromfield (1977)
C = Crittenden (1973)

others (1973) are about 34 Ma for the eastern stocks, Keetley volcanics and the Clayton

Peak stock; 32 Ma for the Alta stock and 26 Ma for the Little Cottonwood stock. Biotite

K/Ar ages are significant for the eastern stocks and the Keetley volcanics because they

represent emplacement ages due to the quenched textures of these rocks. Zircon U/Pb

ages with a closing temperature of 750° (Feher et al., 1996) represent emplacement ages

as well and were determined to be 36 Ma for Clayton Peak stock, 33.5 Ma for the Alta

stock and 30.4 Ma for the Little Cottonwood stock.

Chemical Compositions and Mineralogy of the Keetley Volcanics

Whole Rock Chemical Compositions of the Keetley Volcanics

A total of 67 chemical analyses were done on the Keetley volcanics. The major

element and trace element analyses from XRF spectroscopy are given in Tables 2 and 3 of

Appendix B. XFR techniques are discussed on p.10. The Keetley volcanics occur mostly

within the high-K calc-alkaline series of rocks (Figure 6) however, they do not follow the

typical AFM, calc-alkaline differentiation trend (Figure 7). The Keetley volcanics have a

large variation in chemical composition which is illustrated in Figure 8. Figure 8 compares

the entire Central Volcanic Zone of the Andes which is composed of several individual

volcanic systems to the single volcanic system of the Keetley volcanics. Most of the

Keetley volcanics span this large variation.

The major element trends of CaO, FeO and MgO in general show decreasing

trends with an increase in SiO_2, but they do not show particularly coherent trends (Figure

9). MgO has the most deviation from a linear trend (Figure 9). The alkalis (Na_2O and

K_2O), Al_2O_3, and TiO_2 show scatter at constant SiO_2 (Figure 9). The trace elements; Rb,
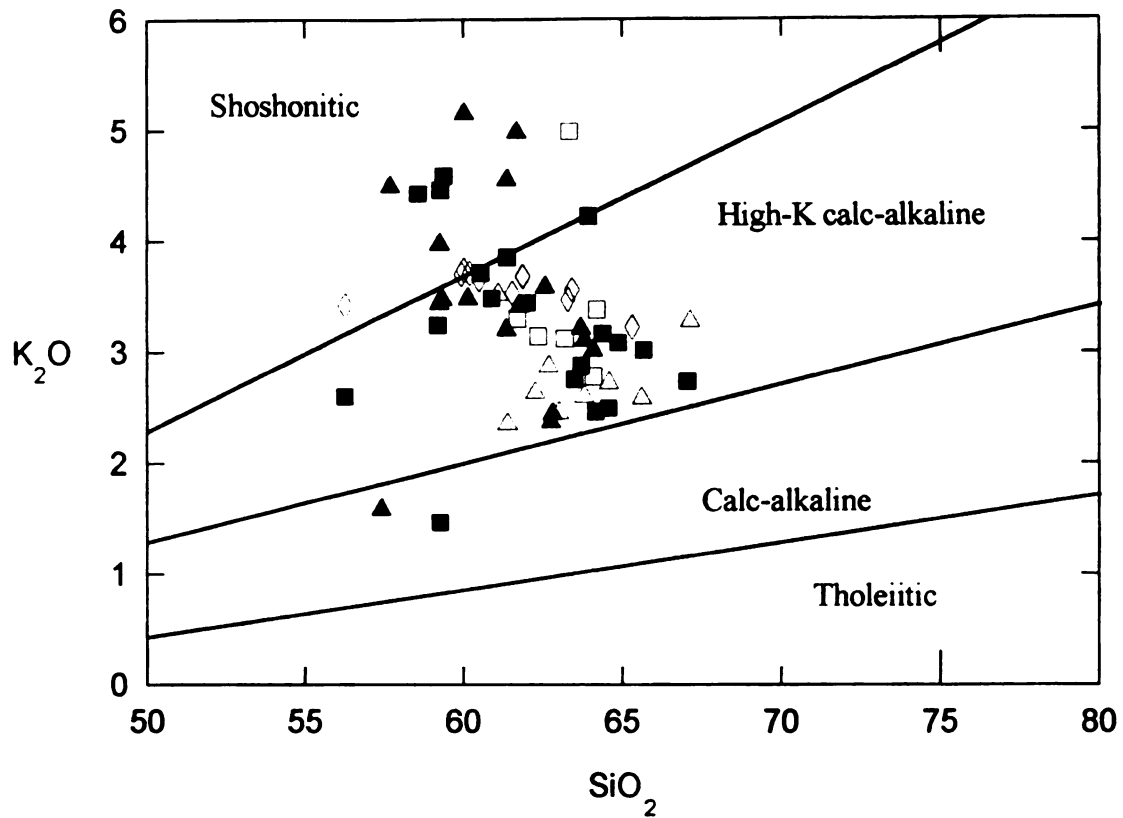
Figure 6. High-K calc-alkaline classification of the Keetley volcanics based
on divisions after McBirney (1993). Symbols for the Keetley volcanics are
filled squares for Jordanelle Dam location, open squares for Francis, open diamonds
for Indian Hollow, filled triangles for Peoa and open triangles for I-80.
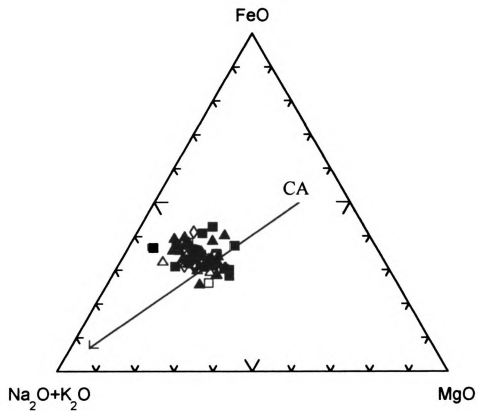
Figure 7. A typical AFM calc-alkaline differentiation trend after Hess (1989) plotted with the chemical trend of the Keetley volcanics. CA = calc-alkaline and the solid black line is the path of differentiation. Symbols for the Keetley volcanics are the same as in Figure 6.
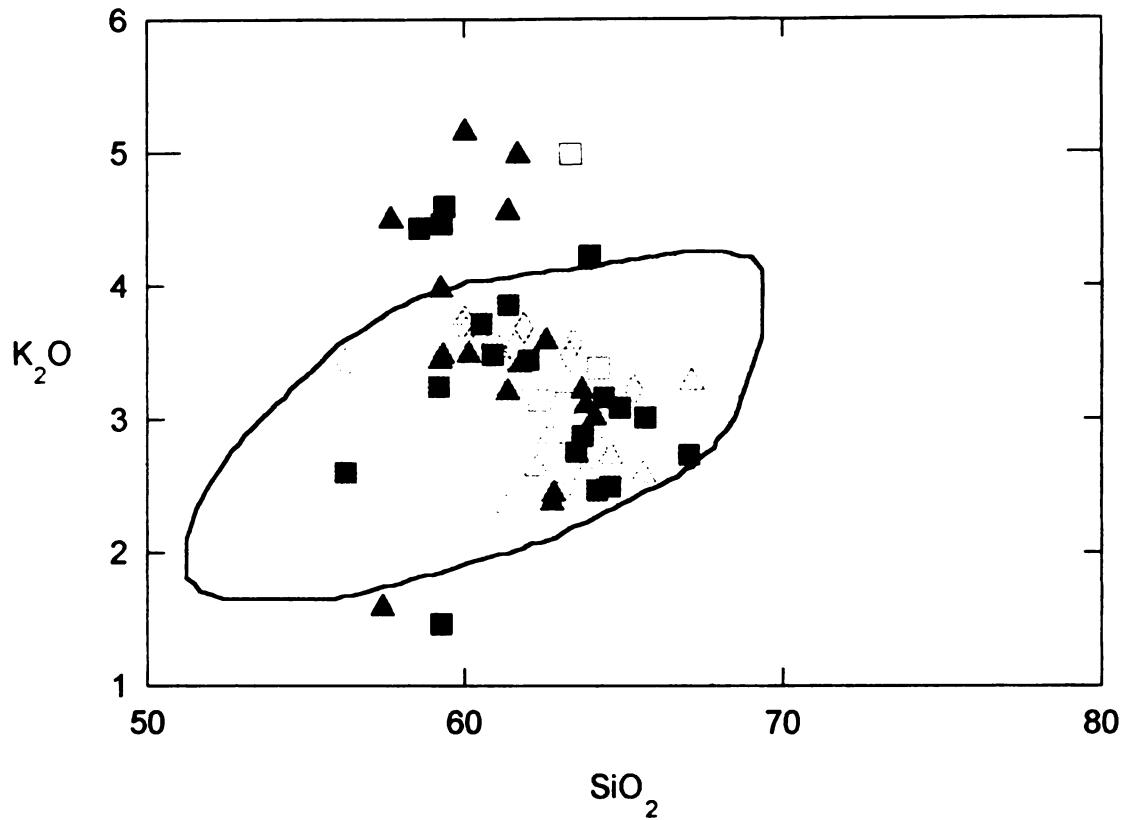
Figure 8. Comparison of high-K calc-alkaline volcanic rocks from the
Central Volcanic Zone (CVZ) of the Andes in northern Chile, north-west
Argentina and south-west Bolivia (shaded area) to the Keetley volcanics.
Data on the CVZ from Wilson (1989). Most of the Keetley volcanics span
the entire compostitional range of the volcanic systems within the high-K
calc-alkaline volcanics from the CVZ. Symbols for Keetley volcanics are the
same as in Figure 6.

Figure 9.   Major element variation diagrams for the Keetley volcanics. Note the large
variation in MgO, TiO_2, Al_2O_3 and the alkalis with a small variation in
SiO_2. Symbols for the Keetley volcanics are the same as in Figure 6.
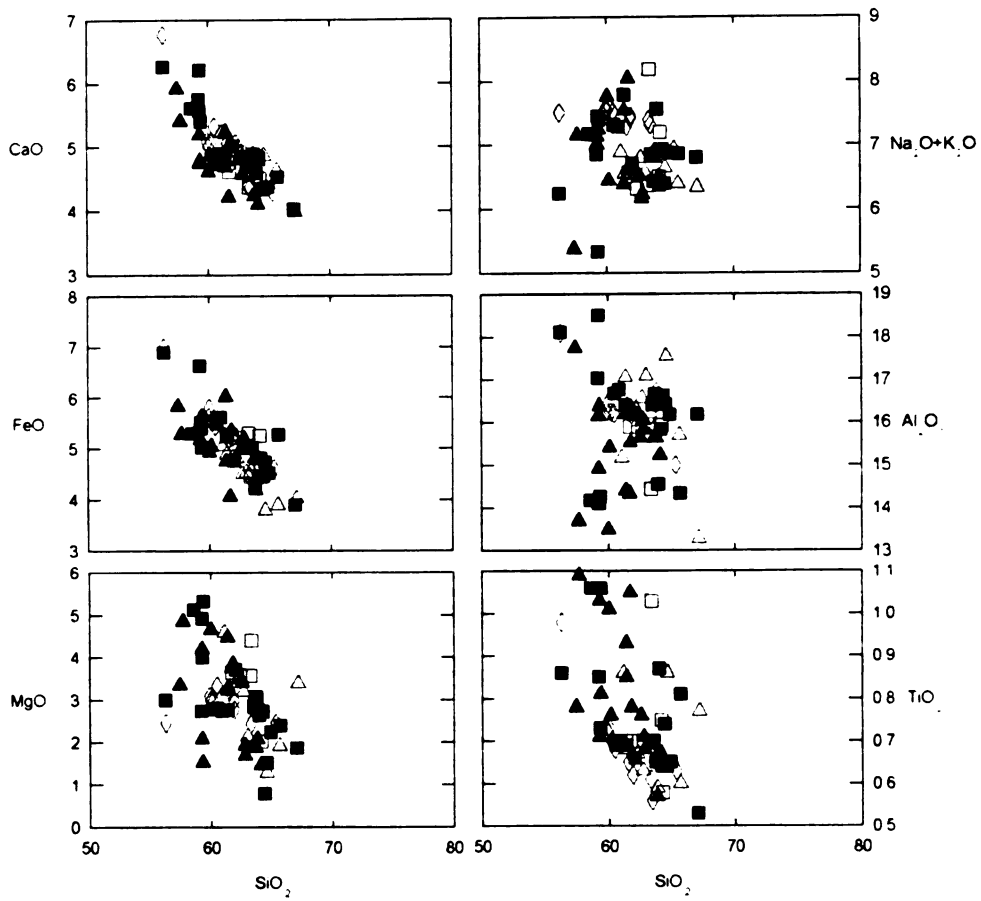
Sr, Ba, Zr, Nb have little coherence at nearly constant SiO_2. P_2O_5 shows a general

decrease with increase in silica but is not a tight linear trend (Figure 10).

Mineralogy of the Keetley Volcanics

Petrography

A total of 50 thin sections were prepared from the volcanic clasts of the

Keetley volcanics. Representative modal analyses for the Keetley volcanics are illustrated

in Table 4. A total of 800 point counts were done for each modal analysis. The

distinction between phenocrysts and matrix was based on grain size. Any grain that was

less than .5 mm was considered matrix and anything larger was considered a phenocryst.

The amount of phenocrysts in the volcanic clasts ranges from 35% to 63% (Table 4), with

a mean percentage of phenocrysts equal to 53.5%. Petrographic descriptions of the

Keetley volcanics will be given collectively due to their similarities. The major variation

being the presence or absence of pyroxene.

The Keetley volcanics are porphyritic andesites. All samples contain phenocrysts

of plagioclase and hornblende as the major phases with minor amounts of biotite in most

samples, with the exception of JD 19-9 and IH 17-13 which contain about 10% biotite

each. In most samples plagioclase is the dominant phenocryst (Table 4). Plagioclase

occurs as medium- to fine-grained, euhedral to subhedral laths as well as microphenocrysts

within the matrix. Plagioclase laths have characteristic oscillatory zoning and many are

reversely zoned. Plagioclase melt inclusions are very common in nearly all of the thin

sections.

Hornblende is the next most abundant phenocryst phase and occurs as fine- to

medium-grained, euhedral to subhedral phenocrysts. Hornblende phenocrysts often

Figure 10.   Trace element variation diagrams for the Keetley Volcanics. All trace elements show scatter at constant SiO_2. Symbols for the Keetley volcanics are the same as in Figure 6.
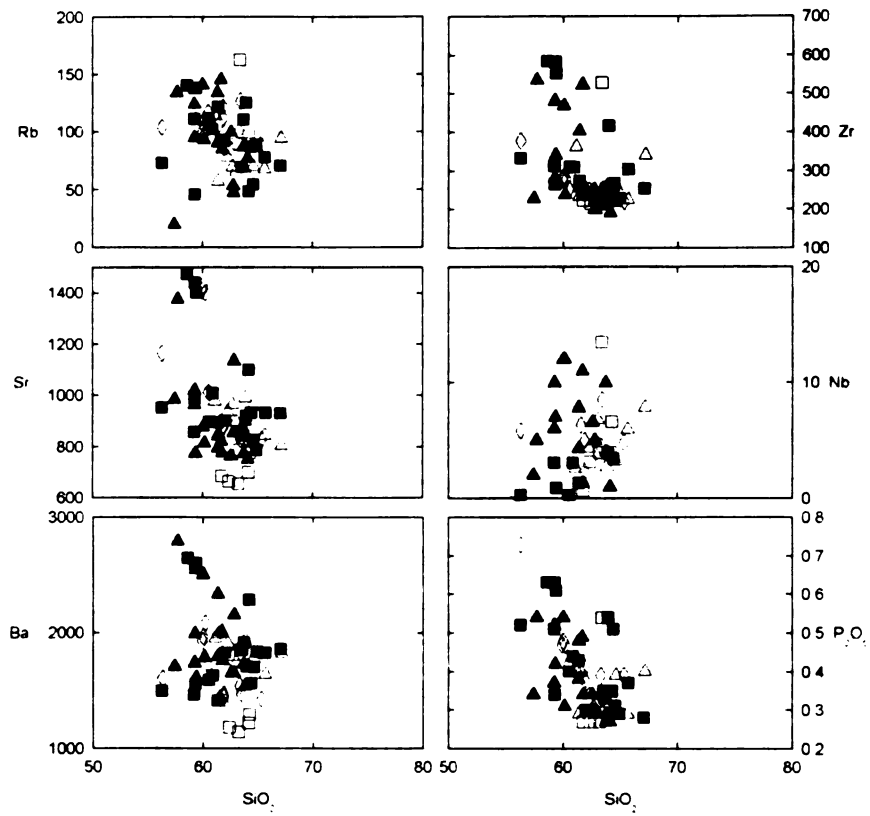
Table 4. Modal point count anlayses shown in percent.

Sample #	Plag	Amph	Biot	Cpx	Opaq	Qtz	Matrix	Phenocrysts
JD 18-8	28.25	11.63	11.25	5.88	0.75	0.63	41.63	58.37
JD 19-9	25.25	3.36	9.95	20.40	2.11	1.24	37.69	62.31
JD 19-10	12.73	3.62	10.24	17.35	2.62	1.87	51.56	48.44
JD 19-17	25.75	8.00	5.50	0.50	0.88	0.00	59.38	40.62
JD 19-1	28.13	9.63	1.38	1.63	8.63	0.00	50.63	49.37
JD 19-2	30.84	16.23	1.37	0.12	1.87	0.00	49.56	50.44
JD 18-9B	19.50	12.00	0.25	0.75	1.75	0.00	65.75	34.25
JD 19-37	34.42	7.29	1.63	0.00	3.39	2.39	50.88	49.12
IH 16-4	20.63	15.63	1.13	1.50	4.88	0.00	56.25	43.75
IH 17-2	32.44	16.15	4.62	0.00	0.90	0.77	45.13	54.87
IH 17-13	12.73	3.62	10.24	17.35	2.62	1.87	51.56	48.44
IH 17-23	23.91	13.70	1.12	1.25	1.49	0.00	58.53	41.47
IH 17-25	24.50	17.25	0.13	1.25	2.50	0.00	54.38	45.62
I-80 15-11	17.98	11.40	2.47	1.18	9.87	1.06	56.05	43.95
I-80 20-14	25.88	13.13	3.75	0.00	4.13	0.63	52.50	47.50
PEOA 19-27	33.29	2.12	0.37	11.85	2.12	0.00	50.25	49.75
PEOA 19-28	32.58	4.24	1.50	14.48	1.12	0.00	46.07	53.93
PEOA 19-31	12.50	1.82	6.19	19.42	2.43	0.00	57.65	42.35
FRAN 20-3	25.06	14.09	1.00	6.23	1.87	0.25	51.75	48.25
FRAN 20-11	25.59	7.24	4.00	16.10	2.62	0.00	44.44	55.56

display oscillatory zoning (Figure 11a-b). Also note the near parallel alignment of the phenocrysts in Figure 11a-b, this texture is most common in the samples from the Indian Hollow location. Occasionally hornblende is cored by pyroxene. Inclusions of plagioclase, opaques and some biotite are common. In most samples the hornblende phenocrysts are surrounded by very fine-grained clinopyroxene (Figures 12a-b and 13a-b). Disequilibrium of hornblende phenocrysts is common and is characterized by reaction rims that are composed of opaques. In some cases the hornblende phenocrysts not only have reaction rims but appear to have been nearly completed reacted to form an opaque mineral (magnetite?). In these same samples the clinopyroxene is in equilibrium and appears fresh and unaltered and does not appear to have reacted (Figure 14a-b).

In about 80% of the samples clinopyroxene exists as fine- to medium-grained, euhedral to subhedral phenocrysts coexisting with hornblende as well as in the matrix as microphenocrysts in most samples. One orthopyroxene phenocryst was detected by electron microprobe and a few phenocrysts were found in thin section.

Biotite exists as phenocrysts and microphenocrysts within the matrix. Biotite phenocrysts are less abundant than hornblende phenocrysts in most samples. They are fine-grained, euhedral to subhedral, and are often nucleated on hornblende phenocrysts. In most of the samples in which hornblende has reacted to opaques the biotite has reacted as well.

Opaque minerals are found in all samples and the majority are magnetite, however, rare grains of illmenite were detected by electron microprobe analysis.

Quartz occurs as anhedral, resorbed, embayed grains up to 1.5 mm in a few samples and does not have a modal abundance of more than about 2.5%. Based on the

Figure 11a-b. Photomicrograph of sample 17-23 IH, in plane polarized light a) and with
crossed polars b). Note oscillatory zoning of hornblende as well as a near
parallel alignment of the phenocrysts. Field of view is 4.4 mm across.
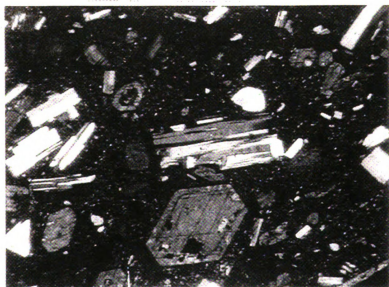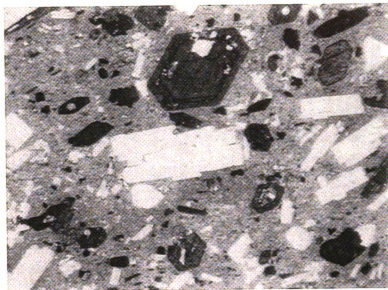
Figure 12a-b. Photomicrograph of sample 20-3 Fran, in plane polarized light a) and with crossed polars b). The hornblende phenocryst is rimmed by smaller grains of clinopyroxene. Note the small grains of clinopyroxene in the matrix. Field of view is 4.4 mm across.
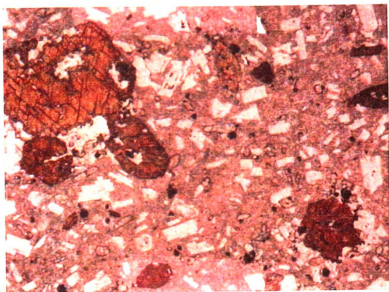
Figure 13a-b. Photomicrograph of sample 20-3 Fran under higher magnification in
plane polarized light a) and with crossed polars b). Note the unaltered
clinopyroxene surrounding the altered/reacted hornblende
phenocryst. Field of view is 1.2 mm across.
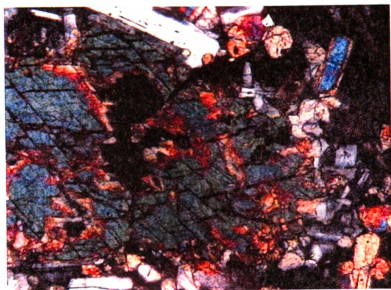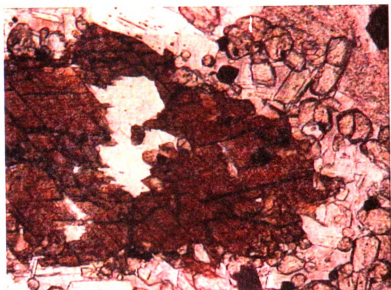
Figure 14a-b. Photomicrograph of sample 19-3b JD, in plane polarized light a) and with
crossed polars b). At the top is a phenocryst of hornblende that has
reacted and is in disequilibrium along side a fresh, unaltered clinopyroxene.
Field of view is 1.2 mm across.
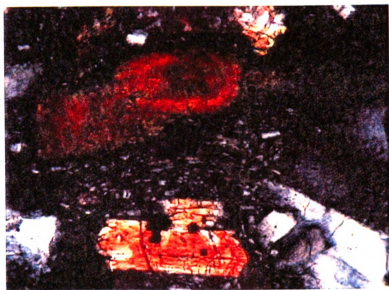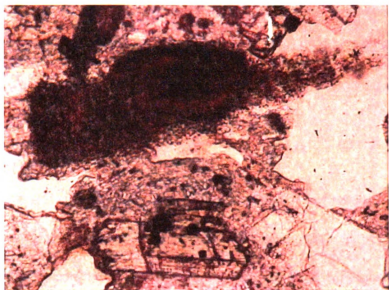
resorbed, embayed texture and the rare occurrence it is probable that the quartz grains are

xenocrysts (Figure 15a-b). However, the texture of these may be due to the fact that the

quartz grains are disequilibrium phenocrysts. One large grain and a few smaller grains of

K-feldspar occur as irregular grains (Figure 16a-b). These are probably xenocrysts. Rare

mineral aggregates up to 1 cm are found throughout the samples and generally are

composed of hornblende, biotite and quartz phenocrysts.

Electron Microprobe Analysis

Mineral chemical compositions were determined by a Cameca Camabax electron

microprobe at the University of Indiana for plagioclase, amphibole, pyroxene, and biotite

(see p. 10-11 for a description of techniques). Magnetite is the dominant opaque mineral.

Representative plagioclase compositions are presented in Table 5. The total range

of plagioclase phenocrysts for all microprobe analyses are illustrated in Figure 17. The

one analysis that is orthoclase is probably a K-feldspar xenocryst. Two analyses are albitic

plagioclase (An_{10}), both of these analyses are rim analyses. Most plagioclase rim

compositions are within An_{30} to An_{53} with a maximum anorthite variation of An_{32} to An_{45}

in sample 19-9. An anomalous variation from An_{10} to An_{45} occurs within sample 19-2

(Figure 18). The plagioclase middle compositions have a maximum anorthite variation of

An_{41} to An_{50}, which occurs within sample 19-2 (Figure 19). The maximum anorthite

variation within the matrix plagioclase ranges from An_{42} to An_{48} and occurs within sample

19-17 (Figure 20). Several of the plagioclase phenocrysts are reversely zoned (Table 5)

and are not specific to any one sample or a group of samples. Examples of reverse zoning

are illustrated in Figure 21. Oscillatory zoned grains are also common.

Figure 15a-b. Photomicrograph of sample 20-18 I-80, in plane polarized light a) and
with crossed polars b). Notice the two grains of quartz on the left and
right-hand sides. Both of these grains exhibit resorbed and embayed
textures.
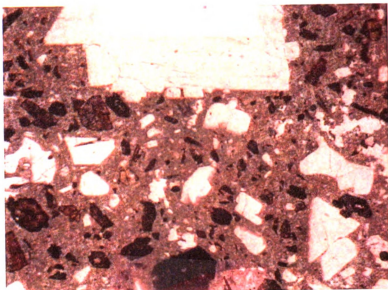
Figure 16a-b.   Photomicrograph of sample 17-2 IH, in plane polarized light a) and
crossed polars b).   A large grain of K-feldspar makes up most of the
field of view.   This grain is probably a xenocryst.
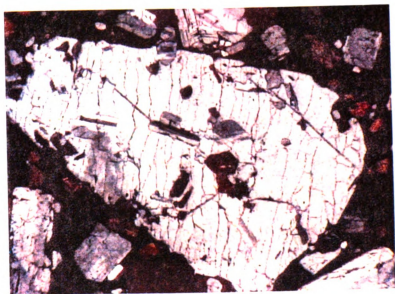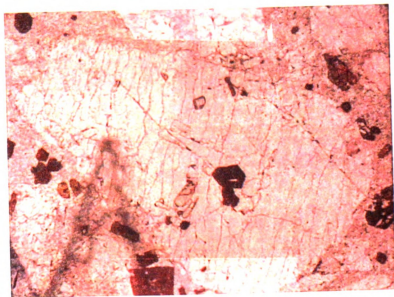
Table 5. Representative plagioclase phenocryst microprobe analyses.

Sample	18-8-4 core	18-8-4 mid	18-8-4 rim	19-37-3 core	19-37-3 mid	19-37-3 rim	19-27-5 core	19-27-5 mid	19-27-5 rim
SiO2	57.65	55.75	56.36	69.38	58.09	57.73	57.67	58.11	56.71
Al2O3	27.50	28.89	27.90	9.82	26.84	26.86	27.33	28.37	27.83
FeO	0.51	0.35	0.44	0.09	0.30	0.16	0.42	0.43	0.59
CaO	9.08	10.81	9.61	1.80	8.44	8.37	8.78	10.21	9.62
Na2O	5.91	5.23	5.86	3.21	6.55	6.71	6.10	5.31	5.75
K2O	0.69	0.53	0.56	1.03	0.34	0.43	0.84	0.59	0.79
Total	101.33	101.56	100.73	85.32	100.55	100.26	101.13	101.02	101.30
Ab	51.91	45.25	50.76	61.09	57.26	57.75	53.00	46.85	49.63
An	44.08	51.71	46.03	36.53	40.77	39.80	42.18	49.75	45.88
Or	4.01	0	3.21	2.38	1.97	2.45	0	3.39	4.49

Sample	19-17-2 core	19-17-2 mid	19-17-2 rim	19-17-5 core	19-17-5 mid	19-17-5 rim	17-24-6 core	17-24-6 mid	17-24-6 rim
SiO2	58.12	57.63	58.55	55.95	57.63	58.06	54.49	57.29	57.78
Al2O3	25.91	26.13	25.90	27.79	25.81	25.11	29.16	26.95	26.18
FeO	0.33	0.29	0.31	0.39	0.40	0.49	0.28	0.29	0.38
CaO	8.05	9.04	8.43	10.12	8.19	7.66	11.69	9.19	8.41
Na2O	6.44	6.14	6.02	5.27	6.21	6.33	4.87	6.07	6.22
K2O	0.73	0.65	0.74	0.46	0.82	0.99	0.30	0.56	0.78
Total	99.58	99.86	99.94	99.98	99.06	98.65	100.77	100.34	99.74
Ab	56.64	53.13	53.92	47.2	55.09	56.45	42.24	52.73	54.66
An	39.13	43.2	41.74	50.12	40.15	37.73	56.03	44.08	40.85
Or	4.23	3.68	4.34	2.68	4.76	5.82	1.73	3.2	4.49

Table 5. continued

Sample	19-28-9 core	19-28-9 mid	19-28-9 rim	16-4-1 core	16-4-1 mid	16-4-1 rim	19-2-5 core	19-2-5 mid	19-2-5 rim
SiO_2	60.636	57.355	57.518	55.749	57.81	55.199	55.131	55.356	56.445
Al_2O_3	24.36	26.055	25.91	27.706	26.365	27.464	28.352	27.634	26.917
FeO	0.439	0.368	0.443	0.293	0.292	0.423	0.328	0.283	0.429
CaO	6.555	8.898	8.107	10.19	8.428	10.102	10.674	10.072	9.358
Na_2O	6.972	6.032	6.199	5.504	6.453	5.272	5.475	5.527	5.953
K_2O	1.408	0.829	0.877	0.379	0.584	0.486	0.276	0.331	0.387
Total	100.37	99.337	99.054	99.821	99.932	98.946	100.236	99.203	99.489
Ab	60.52	52.99	55.07	48.35	56.14	47.18	47.38	48.86	52.32
An	31.44	42.22	39.8	49.46	40.52	49.96	51.04	49.21	45.44
Or	8.04	4.79	5.12	2.19	3.34	2.86	1.57	1.93	2.24
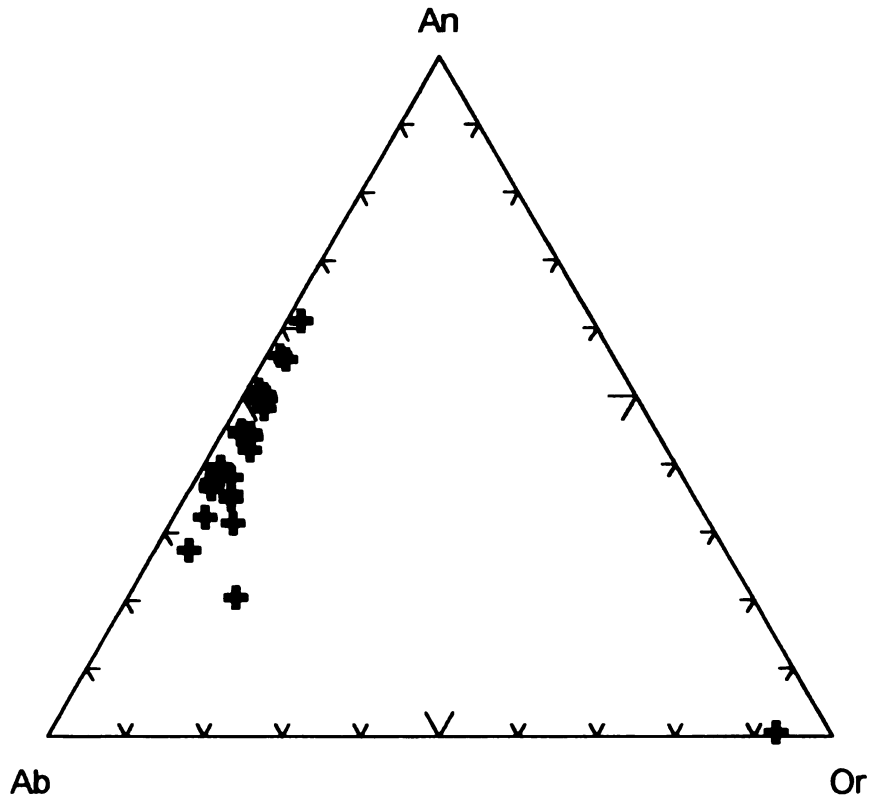
Figure 17. Feldspar triangle including rim, middle and matrix plagioclase phenocryst compositions. The one analysis at the Or apex is a K-feldspar xenocryst.

Figure 18.   Anorthite variations within plagioclase rim analyses. Diamonds are the maximum % An and the squares are the minimum % An within each sample.
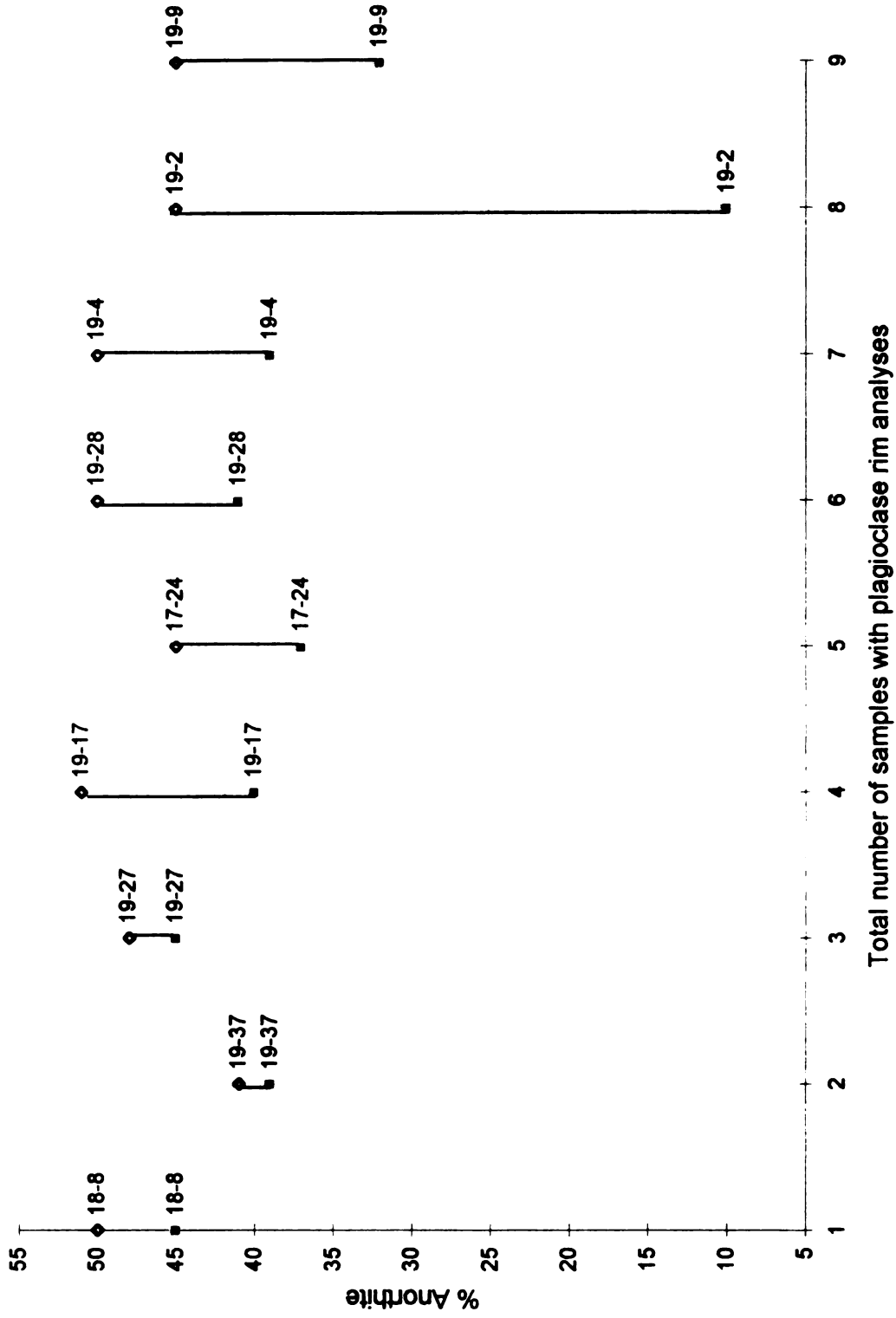
Figure 19.   Anorthite variations within plagioclase middle analyses. Diamonds are the maximum % An and the squares are the minimum % An within each sample.

Figure 20.   Anorthite variations within matrix plagioclase analyses. Diamonds are
the maximum % An and the squares are the minimum % An within each
sample.
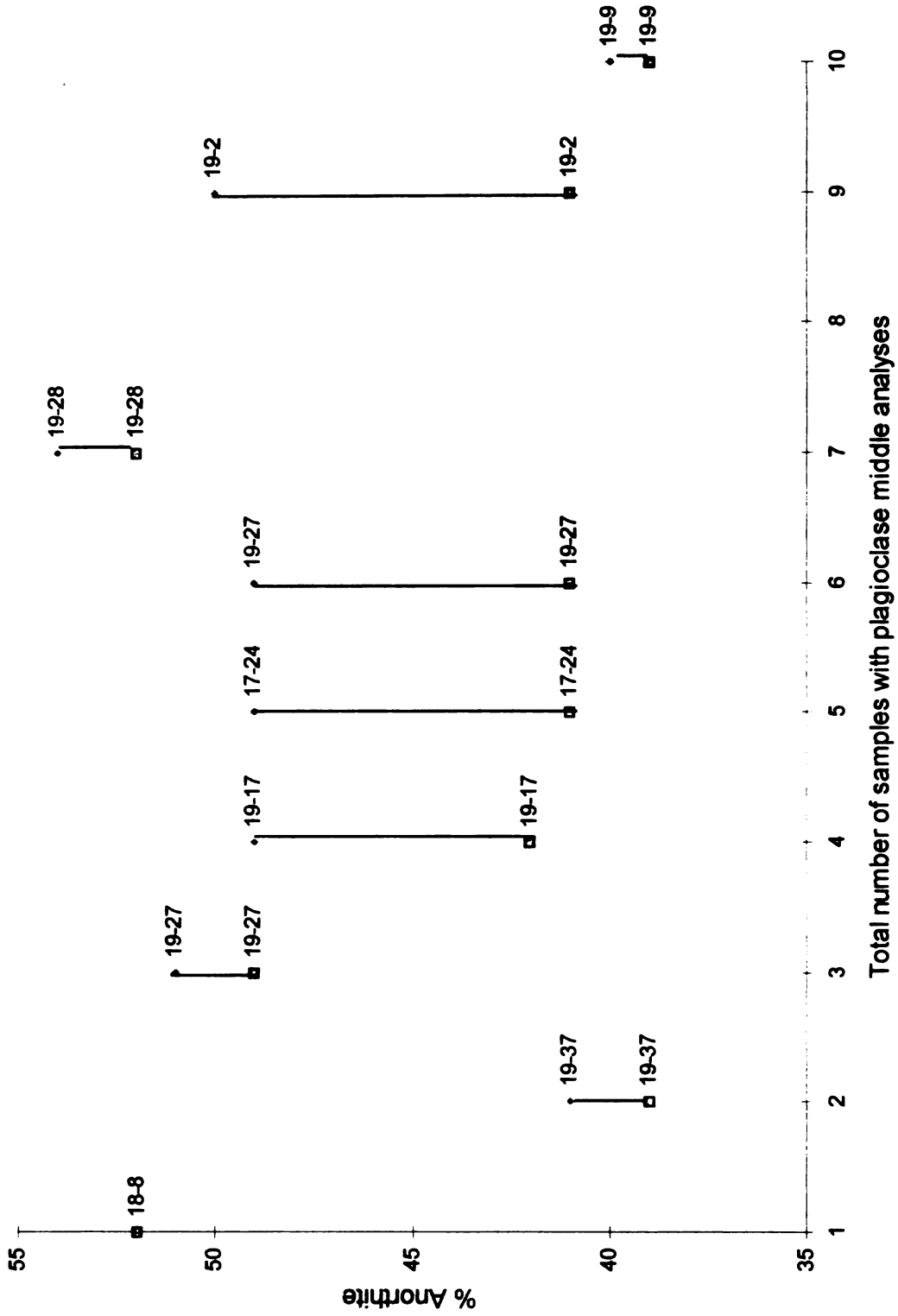
% Anorthite
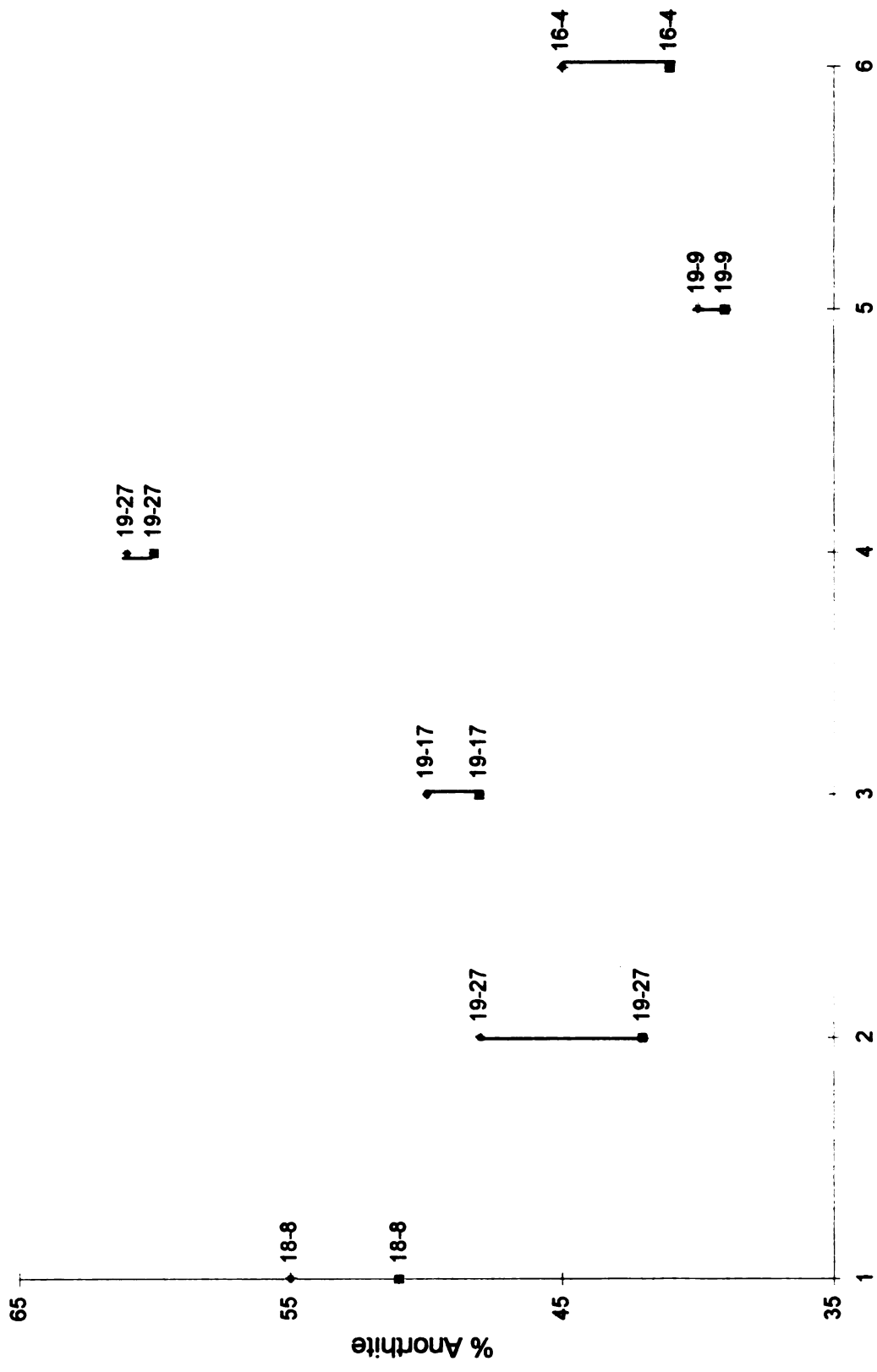
Total number of samples with matrix plagioclase analyses
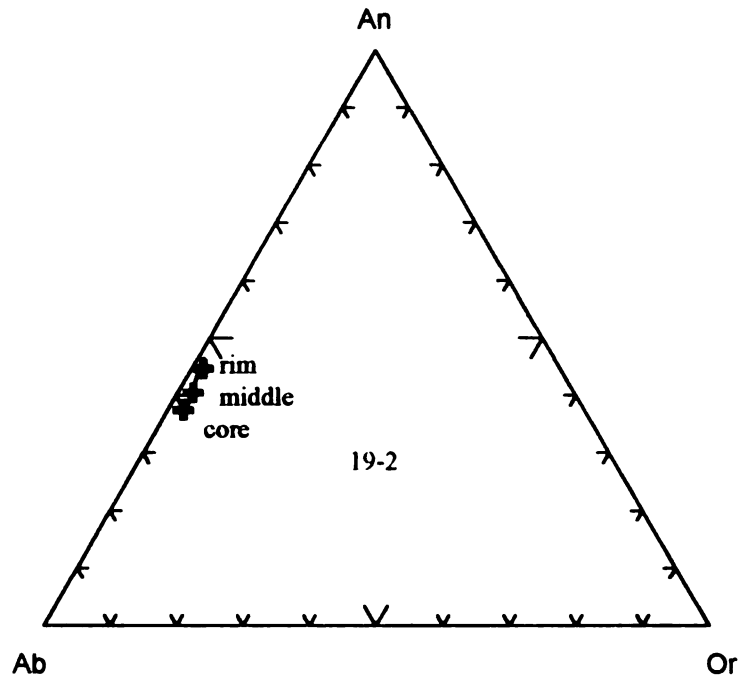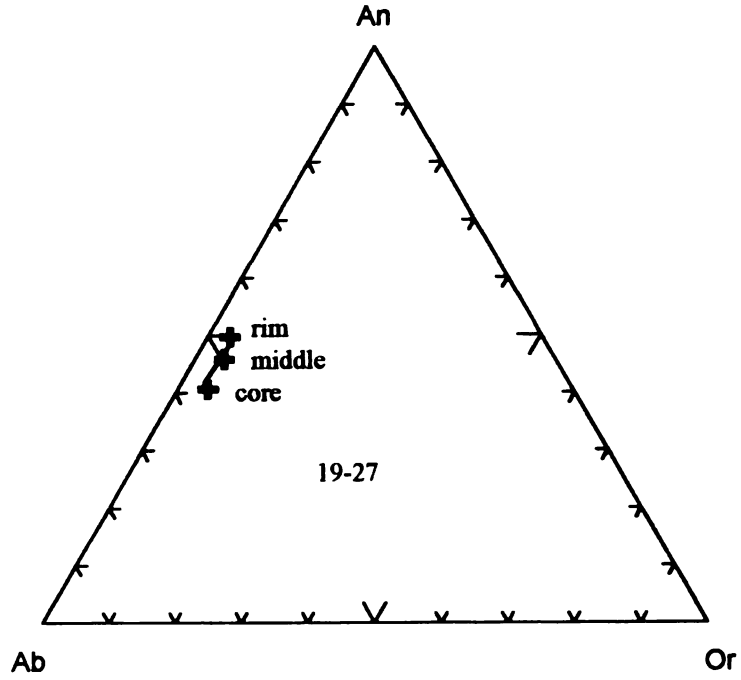
Figure 21. Feldspar triangles showing reverse zoned plagioclase phenocrysts of two representative samples.

Representative amphibole compositions are listed in Table 6. In all of the analyses FeO is calculated as $FeO = FeO + .8998*Fe_2O_3$. The most variation within the amphibole analyses is within MgO, which varies from 9.85% to 14.82%, CaO ranges from 10.75% to 11.95%, with two anomalous analyses at about 20%.

All pyroxene microprobe analyses are plotted in Figure 22 on the pyroxene quadrilateral and representative pyroxene compositions are illustrated in Table 7. Most of the analyses are MgO rich with intermediate CaO and fall within the clinopyroxene range. Three analyses are within the orthopyroxene range. Sample 19-28 is the only sample which allows for two-pyroxene thermometry to be estimated because it contains both clinopyroxene and orthopyroxene.

Table 8 lists some representative compositions of biotite phenocrysts. There is very little variation within the biotite compositions. K_2O is consistent ranging from 8.19 to 9.43 wt. %.

Pyroxene Thermometry

Two-pyroxene thermometry was done using one orthopyroxene analysis with two different clinopyroxene analyses from within sample 19-28 JD. The results of this are illustrated in Table 9. The Ca-QUILF system developed by Lindsley and Frost (1992) was used to determine the temperatures. This method requires that four phases of the FeO-MgO-CaO-TiO_2-SiO_2 system be used. However, only the clinopyroxene and orthopyroxene analyses were available from sample 19-28 JD, no Fe-Ti oxide analyses were obtained. Because of this, reasonable pressures had to be estimate for the clinopyroxene and orthopyroxene compositions in order to obtain temperatures. Using the QUILF program (Anderson et al., 1993) pressures of 1, 2, 4 and 6 Kb were arbitrarily

Table 6. Representative amphibole phenocryst microprobe analyses

Sample	18-8-3 core	18-8-3 mid	18-8-3 rim	17-2-3 core	17-2-3 mid	17-2-3 rim	17-13 core	17-13 mid	17-13 rim
SiO_2	42.83	42.21	41.70	43.36	43.32	76.94	38.56	38.31	38.77
TiO_2	2.85	3.02	2.69	1.87	1.87	0.13	2.84	2.88	2.80
Al_2O_3	10.98	10.68	11.23	9.55	9.64	13.60	13.99	14.11	13.22
FeO	13.17	13.29	12.88	18.14	18.32	0.40	13.98	14.17	17.47
MnO	0.32	0.28	0.34	0.45	0.44	0.00	0.15	0.17	0.41
MgO	13.82	13.78	13.93	11.18	11.03	0.02	12.10	12.13	9.85
CaO	11.40	11.27	11.69	11.18	11.49	0.59	11.95	11.80	11.67
Na_2O	2.11	2.17	2.14	1.79	1.75	0.74	1.54	1.55	1.85
K_2O	1.14	1.19	1.04	1.13	1.19	4.19	1.97	1.98	1.95
H_2O	2.01	2.01	1.99	1.95	1.96	2.37	1.97	1.98	1.95
F	0.00	0.00	0.02	0.00	0.00	0.01	0.00	0.00	0.00
Cl	0.08	0.05	0.06	0.17	0.16	0.03	0.02	0.01	0.07
Total	100.71	99.95	99.71	100.77	101.17	99.02	99.07	99.09	100.01

Sample	19-37-6 core	19-37-6 mid	19-37-6 rim	16-4-4 core	16-4-4 mid	16-4-4 rim
SiO_2	41.44	41.45	41.61	41.08	40.66	41.75
TiO_2	1.52	1.60	1.79	2.14	2.39	2.27
Al_2O_3	11.93	11.82	12.07	11.81	12.67	11.21
FeO	17.60	17.42	17.09	15.73	16.48	15.98
MnO	0.38	0.42	0.41	0.32	0.35	0.37
MgO	10.98	10.83	10.95	11.67	11.51	11.45
CaO	11.60	11.54	11.31	11.72	11.49	11.67
Na_2O	1.76	2.34	2.28	2.18	2.17	2.03
K_2O	1.38	1.36	0.79	1.03	1.38	1.40
H_2O	1.93	1.95	1.98	2.00	2.00	1.97
F	0.00	0.00	0.00	0.00	0.00	0.00
Cl	0.22	0.15	0.07	0.11	0.02	0.09
Total	100.74	100.88	100.35	99.79	101.12	100.19

Wo_{50}

En

Fs
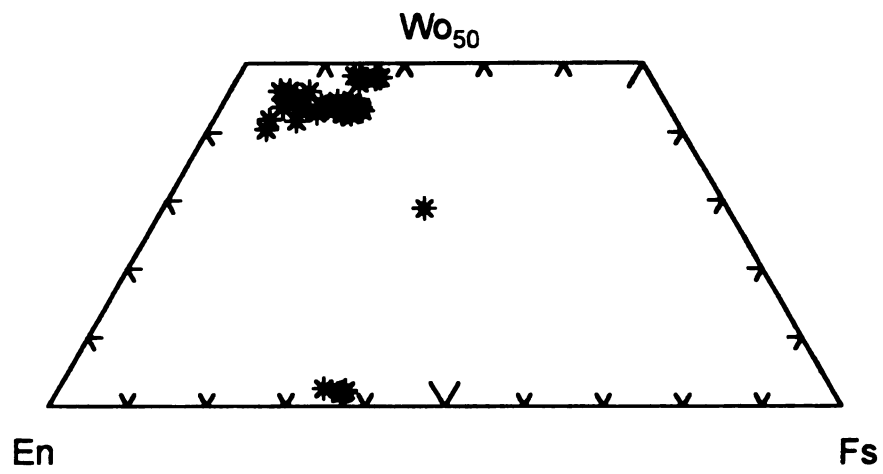
Figure 22. Simple pyroxene quadrilateral including all pyroxene phenocryst compostions including rims, cores and middles.

Table 7. Representative pyroxene phenocryst microprobe analyses.

Sample	18-8-1 core	18-8-1 mid	18-8-1 rim	19-28-4 core	19-28-4 mid	19-28-4 rim	16-4-3 core	16-4-3 mid	16-4-3 rim
SiO_2	51.63	51.24	51.24	51.89	52.15	49.44	52.57	52.16	50.81
TiO_2	0.37	0.42	0.42	0.17	0.17	0.74	0.28	0.40	0.48
Al_2O_3	2.13	2.26	2.26	1.60	1.44	4.10	1.41	2.09	2.60
FeO	8.68	9.16	9.16	10.41	10.09	9.55	4.01	4.71	6.27
MnO	0.48	0.58	0.58	0.39	0.45	0.16	0.11	0.12	0.19
MgO	14.65	14.18	14.18	13.88	14.16	14.40	17.21	16.79	15.86
CaO	21.53	21.07	21.07	21.24	21.42	20.76	23.12	23.16	23.00
Na_2O	0.37	0.52	0.52	0.53	0.44	0.36	0.30	0.34	0.33
Total	99.84	99.43	99.43	100.09	100.32	99.50	99.02	99.75	99.55
En	43.25	43.00	42.67	41.39	41.73	44.14	49.72	48.93	47.41
Fs	11.06	11.64	11.73	13.08	12.89	10.11	2.28	4.98	13.18
Wo	45.69	45.36	45.59	45.53	45.39	45.74	48.01	48.51	49.41

Sample	19-9-5 core	19-9-5 mid	19-9-5 rim	19-17-1 core	19-17-1 mid	19-17-1 rim	17-13 core	17-13 mid	17-13 rim
SiO_2	53.66	54.14	52.63	51.76	51.55	51.23	48.05	45.44	46.19
TiO_2	0.29	0.23	0.50	0.30	0.43	0.52	0.51	1.16	1.15
Al_2O_3	0.91	0.74	1.66	2.16	2.57	2.89	2.23	6.02	6.53
FeO	4.76	4.52	7.88	4.87	5.09	5.44	8.61	10.20	10.54
MnO	0.10	0.08	0.34	0.15	0.06	0.16	0.43	0.42	0.17
MgO	19.17	18.54	15.93	17.41	16.97	16.41	14.80	12.74	11.36
CaO	20.61	21.08	21.24	21.82	22.01	22.25	22.98	22.62	22.24
Na_2O	0.28	0.25	0.39	0.41	0.41	0.34	0.44	0.50	0.55
Total	99.77	99.57	100.36	98.87	99.09	99.03	99.04	99.08	98.73
En	54.11	51.78	46.13	51.47	50.37	49.61	45.25	39.42	37.69
Fs	4.08	5.88	9.67	2.15	2.65	4.02	5.79	6.21	9.29
Wo	41.81	42.34	44.20	46.38	46.98	47.37	48.95	54.37	53.02

Table 8. Representative biotite phenocryst microprobe analyses.

Sample	17-2-5 core	17-2-5 rim	19-37-1 core	19-37-1 rim	19-2-1 core	19-2-1 rim	19-9-2 core	19-9-2 rim	19-37-5 core	19-37-5 rim
SiO_2	36.94	35.68	35.48	35.10	36.83	35.91	36.49	35.76	34.79	35.67
TiO_2	4.55	4.71	3.96	3.90	3.66	4.28	4.17	6.94	4.08	4.11
Al_2O_3	14.65	14.11	14.77	14.29	14.86	14.62	14.78	14.18	14.66	14.40
FeO	17.90	20.08	19.36	19.71	15.18	14.50	11.78	13.08	19.98	20.30
MnO	0.10	0.19	0.12	0.23	0.13	0.20	0.13	0.05	0.16	0.15
MgO	12.70	11.88	11.92	11.70	15.48	15.61	18.00	15.52	11.87	12.08
CaO	0.07	0.04	0.05	0.02	0.07	0.07	0.02	0.02	0.08	0.00
Na_2O	0.35	0.48	0.48	0.53	0.74	0.79	0.79	0.79	0.54	0.49
K_2O	9.43	9.22	8.99	9.05	8.38	8.19	8.82	8.43	8.75	9.00
H_2O	3.69	3.57	3.39	3.55	3.80	3.50	3.31	2.89	3.52	3.54
F	0.57	0.70	1.01	0.55	0.40	0.95	1.52	2.33	0.68	0.73
Cl	0.15	0.15	0.17	0.19	0.13	0.09	0.07	0.06	0.14	0.19
Total	101.10	100.80	99.69	98.82	99.67	98.71	99.87	100.07	99.24	100.66

used and the resulting temperatures were then determined for each pressure using the calculated end members of the pyroxenes (Table 9). For Group 1 and 2 pyroxenes the lowest average temperatures at which orthopyroxene are in equilibrium with clinopyroxene are at 1 Kb = 1130 °C, at 2 Kb = 1132 °C, at 4 Kb = 1137 °C and at 6 Kb = 1142 °C.

Hornblende Geobarometry

The total aluminum (Al^T) content of hornblende is pressure sensitive and can be used as a geobarometer if it is in equilibrium with the assemblage; biotite, plagioclase, sanidine, quartz, sphene, ilmenite or magnetite, melt and possibly vapor (Hammerstrom and Zen, 1986). This method recalculates Al^T from hornblende formulas on the basis of 23 oxygens and all iron as FeO. The result is a linear relationship between increasing Al^T and increasing pressure. Hammerstrom and Zen (1986) achieved the linear relationship with a correlation coefficient of $r^2 = 0.8$ and an uncertainty of ± 3 kb. This correlation coefficient was refined by Hollister et al. (1987) by analyzing calc-alkaline plutons with intermediate compositions to those used by Hammerstrom and Zen (1986). The result was a $r^2 = .97$ with a reduction in the uncertainty to ± 1 kb. Often the correct mineral assemblage, as listed above, is not available to get accurate estimates of pressure. In a study done by Johnson and Rutherford (1989), the correct mineral assemblage was available for pressure estimates. If the correct mineral assemblage is not available, for example if quartz and sanidine are missing, it is possible to do estimates on samples in which the melt contains greater than 76% SiO_2 and 5% K_2O (anhydrous), which are close to quartz and sanidine saturation (Johnson and Rutherford, 1989). The Keetley volcanics are lacking quartz and sanidine as primary phases and it is not possible to determine the

Table 9. Temperatures estimated from two-pyroxene thermometry based on end-member compositions.

Group 1		Group 2	
Pressure	Temperature	Pressure	Temperature
1 Kbar	1123 °C	1 Kbar	1136 °C
2 Kbar	1126 °C	2 Kbar	1138 °C
4 Kbar	1130 °C	4 Kbar	1143 °C
6 Kbar	1135 °C	6 Kbar	1148 °C

c = core anlaysis, r = rim analysis

End-member compositions for pyroxenes					
Group 1	19-28-3 opx	19-28-5 cpx-c	Group 2	19-28-3 opx	19-28-5 cpx-r
En	64.21	43.25	En	64.21	41.13
Fs	33.41	11.16	Fs	33.41	13.16
Wo	2.38	45.59	Wo	2.38	45.71

composition of the melt because of the non-glassy texture of the groundmass. Therefore the estimate of geobarometry should be used with caution. However, The CIPW norm calculations of the Keetley volcanics are very close to the CIPW norm of the Fish Canyon Tuff (Table 10). Therefore, this method at least provides some sort of estimate for pressure estimates at which hornblende was stable. Using the pressure estimate equation from Johnson and Rutherford (1989);

$$P = (4.09 +/- 0.27) (Al^T) - (3.29 +/- 0.45), \text{ with } r^2 = .96,$$

the low pressure estimate using $Al^T = 1.62$ is $P = 3.35$ Kb, the high pressure estimate using $Al^T = 2.42$ is $P = 6.61$ Kb. The total range of wt.% Al_2O_3 in hornblende is from 9.55 % to 14.11 %.

Assimilation and Fractional Crystallization Models

Table 11 illustrates the results from assimilation and fractional crystallization (AFC) models from the program Mixing (Carr, 1994) after Bryan et al., (1969) in which the sum of the squares of the residuals is calculated by multiple linear regression. The whole rock compositions of the most mafic (18-8 JD) and the most silicic (16-04 Fran, 15-11 IH and 19-37 JD) end-members were chosen as the mixing magmas. Sample 17-31 was chosen as the hybrid because it has an intermediate compositions. Amphibole, plagioclase and clinopyroxene microprobe analyses from 18-8 JD were chosen as the fractionating phases. Sample 18-8 JD was mixed individually with each of the silicic end-member samples and had fractional crystallization of the mafic phases superimposed on the mixing process. The percents of fractionating phases and amounts of end-members necessary for each combination to produce the hybrid magma are listed in Table 11.

Table 10. Comparison of whole rock CIPW norm calculations of the Keetley volcanics vs. the Fish Canyon Tuff. Keetley volcanic samples are those used to calculate hornblende geobarometry.

	FCT 9	17-2 IH	19-37 JD	17-13 IH
QTZ	13.12	14.48	21.60	2.59
OR	23.99	21.03	15.99	20.18
AB	34.19	31.80	34.13	34.55
AN	16.21	16.75	17.66	20.87
DI	1.50	2.26	0.27	6.51
HY	0.00	8.87	5.80	8.18
MT	0.00	2.99	2.92	3.59
ILM	1.14	1.06	1.00	1.86
AP	0.00	0.76	0.64	1.69

Table 11. Multiple linear regression models of Assimilation and Fractional Crystallization for the Keetley volcanics.

Hybrid lava is 17-31 IH

Coef	% Cum	Mineral or Rock
-0.016	-1.616	18-8-3 hbl
-0.036	-3.736	18-8-8 plag
-0.027	-2.827	18-8-1 cpx
0.426	42.9	18-8 JD
0.646	65.1	16-04 IH

Min/Rock	SiO2	TiO2	Al2O3	FeO	MnO	MgO	CaO	Na2O	K2O	P2O5
18-8-3	44.01	2.92	11.13	13.53	0.32	14.2	11.72	2.17	0	0
18-8-8	60.58	0	29.12	0	0.49	0	0	9.81	0	0
18-8-1	51.72	2.14	0.37	14.68	8.69	0.48	21.57	0.37	0	0
18-8JD	57.25	0.87	18.43	7.02	0.14	3.04	6.37	3.7	2.65	0.53
16-04IH	65.52	0.63	15.05	4.63	0.06	2.47	4.3	3.72	3.23	0.39

Hybrid 17-31IH

	SiO2	TiO2	Al2O3	FeO	MnO	MgO	CaO	Na2O	K2O	P2O5
Obs-P	62.17	0.66	16.38	5.24	0.1	2.79	4.78	3.76	3.7	0.41
Calc-P	62.4	0.68	16.33	5.37	-0.16	2.65	4.72	3.58	3.21	0.48
Diff^wt	-0.09	-0.01	0.03	-0.12	0.26	0.14	0.06	0.18	0.48	-0.07

Sum of squares of residuals =.387

Hybrid lava is 17-31IH

Coef	% Cum	Min/Rock
-0.056	-5.656	18-8-3 hbl
-0.024	-2.424	18-8-4 plag
-0.022	-2.222	18-8-1 cpx
0.458	46.1	15-11 I-80
0.638	64.2	18-8 JD

	SiO2	TiO2	Al2O3	FeO	MnO	MgO	CaO	Na2O	K2O	P2O5
18-8-3	44.01	2.92	11.13	13.53	0.32	14.2	11.72	2.17	0	0
18-8-4	60.86	0	29.03	0	0.54	0	0	9.58	0	0
18-8-1	51.72	2.14	0.37	14.68	8.69	0.48	21.57	0.37	0	0
15-11I-	67.54	0.77	13.37	4.05	0.07	3.41	4	3.09	3.29	0.4
18-8JD	57.25	0.87	18.43	7.02	0.14	3.04	6.37	3.7	2.65	0.53

Hybrid 17-31IH

	SiO2	TiO2	Al2O3	FeO	MnO	MgO	CaO	Na2O	K2O	P2O5
Obs-P	62.17	0.66	16.38	5.24	0.1	2.79	4.78	3.76	3.7	0.41
Calc-P	62.39	0.7	16.55	5.26	-0.1	2.7	4.77	3.42	3.19	0.52
Diff^wt	-0.09	-0.04	-0.08	-0.01	0.2	0.1	0.01	0.34	0.5	-0.11

Sum of squares of the residuals = .446

Table 11 (cont.)

Hybrid lava 17-31 IH

Coef	%Cum	Min/Rock
-0.007	-0.707	18-8-3 hbl
-0.098	-9.998	18-8-4 plag
-0.041	-4.141	18-8-1 cpx
0.518	52.4	18-8 JD
0.617	62.4	19-37 JD

Sample	SiO2	TiO2	Al2O3	FeO	MnO	MgO	CaO	Na2O	K2O	P2O5
18-8-3	44.01	2.92	11.13	13.53	0.32	14.2	11.72	2.17	0	0
18-8-4	60.86	0	29.03	0	0.54	0	0	9.58	0	0
18-8-1	51.72	2.14	0.37	14.68	8.69	0.48	21.57	0.37	0	0
18-8JD	57.25	0.87	18.43	7.02	0.14	3.04	6.37	3.7	2.65	0.53
19-37JD	66.6	0.53	16.07	3.87	0.05	1.85	4	4.04	2.71	0.28

Hybrid 17-31IH

	SiO2	TiO2	Al2O3	FeO	MnO	MgO	CaO	Na2O	K2O	P2O5
Obs-P	62.17	0.66	16.38	5.24	0.1	2.79	4.78	3.76	3.7	0.41
Calc-P	62.39	0.67	16.53	5.34	-0.31	2.6	4.81	3.45	3.04	0.45
Diff*wt	-0.09	-0.01	-0.07	-0.09	0.41	0.19	-0.03	0.31	0.65	-0.03

Sum of squares of the residuals = .749

DISCUSSION

Chemical and Age Relationships Between the Keetley Volcanics and the Wasatch Intrusive Belt

Overall there are three and possibly four main chemical groups that characterize the Wasatch Intrusive Belt and the Keetley volcanics (Vogel, in preparation, 1997). The Little Cottonwood stock ranges in silica from 65% to 73%, the Alta stock is intermediate ranging from 60% to 68% silica, and the Clayton Peak stock is the most mafic ranging from 54%-62% silica and they have distinct Rb/Sr - oxide trends. The chemical compositions of the eastern stocks are distinctly different from the Little Cottonwood and Clayton Peak stocks but do have similarities to the Alta stock (Figure 23). The Keetley volcanics are variable but have similarities to the eastern stocks and the Alta stock (Figure 24). The eastern stocks and the Keetley volcanics have biotite K/Ar ages of about 34 Ma. The Alta stock has a zircon U/Pb age of 33.5 Ma. The similarities in the chemical composition and emplacement ages of the Alta stock, eastern stocks and the Keetley volcanics are interpreted to mean that they may be genetically related. Detailed zircon U/Pb (Constenius, pers. comm.,1996), and $^{40}Ar/^{39}Ar$ dating of minerals (Flood, pers. comm., 1996) are in progress to evaluate this suggestion, and to further document the emplacement history and petrologic relationships among the Wasatch intrusive belt.

Evaluation of the effects of P_{H2O} on the evolution of the Keetley Volcanics

Change in pressure can account for the breakdown of hornblende in the Keetley volcanics. The presence of hornblende in disequilibrium in the majority of the samples

61
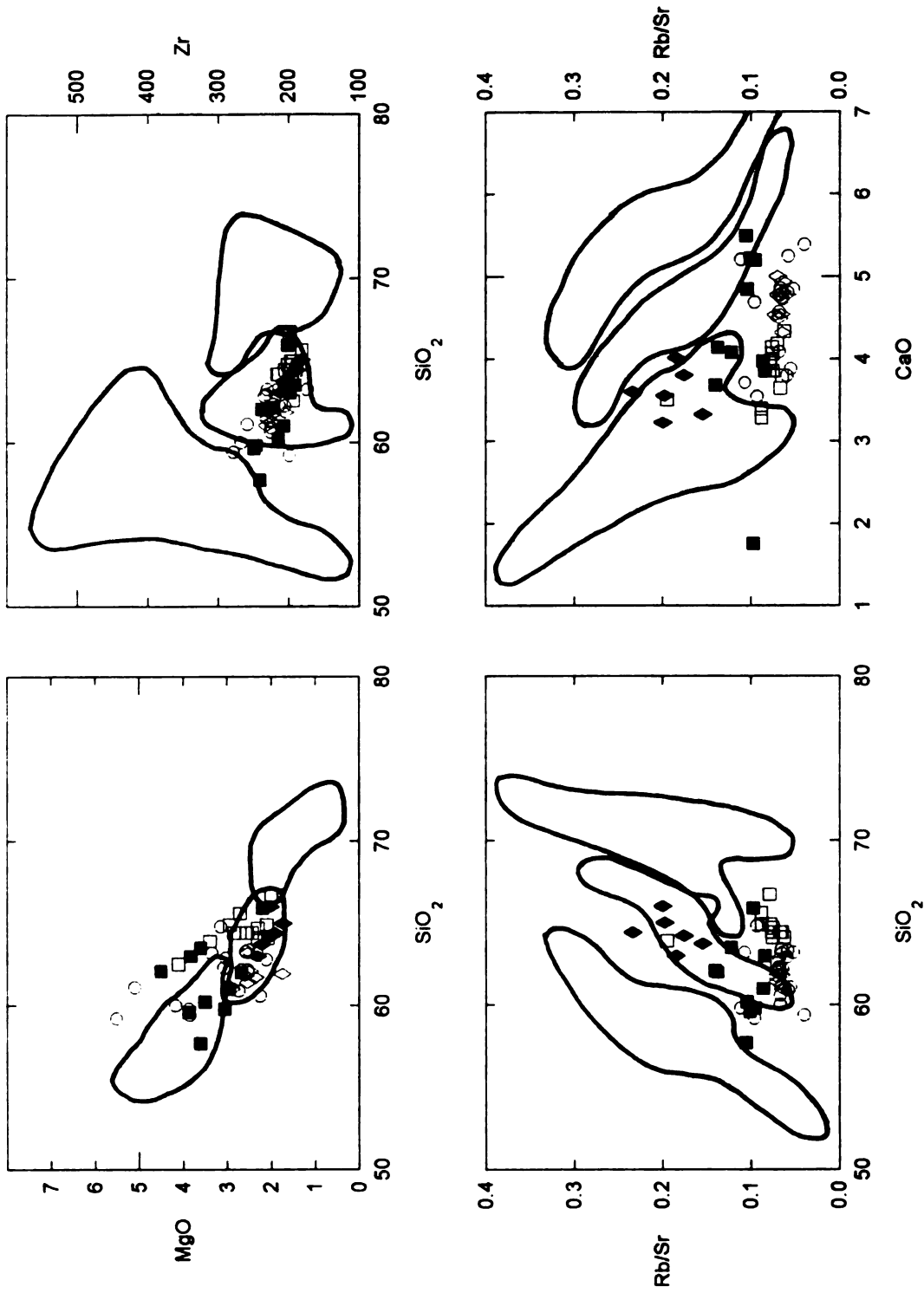
Figure 23. Comparison of the chemical compositions of the Western stocks (superimposed areas) to the Eastern Stocks. Symbols for the Eastern stocks are the same as in Figure 5.
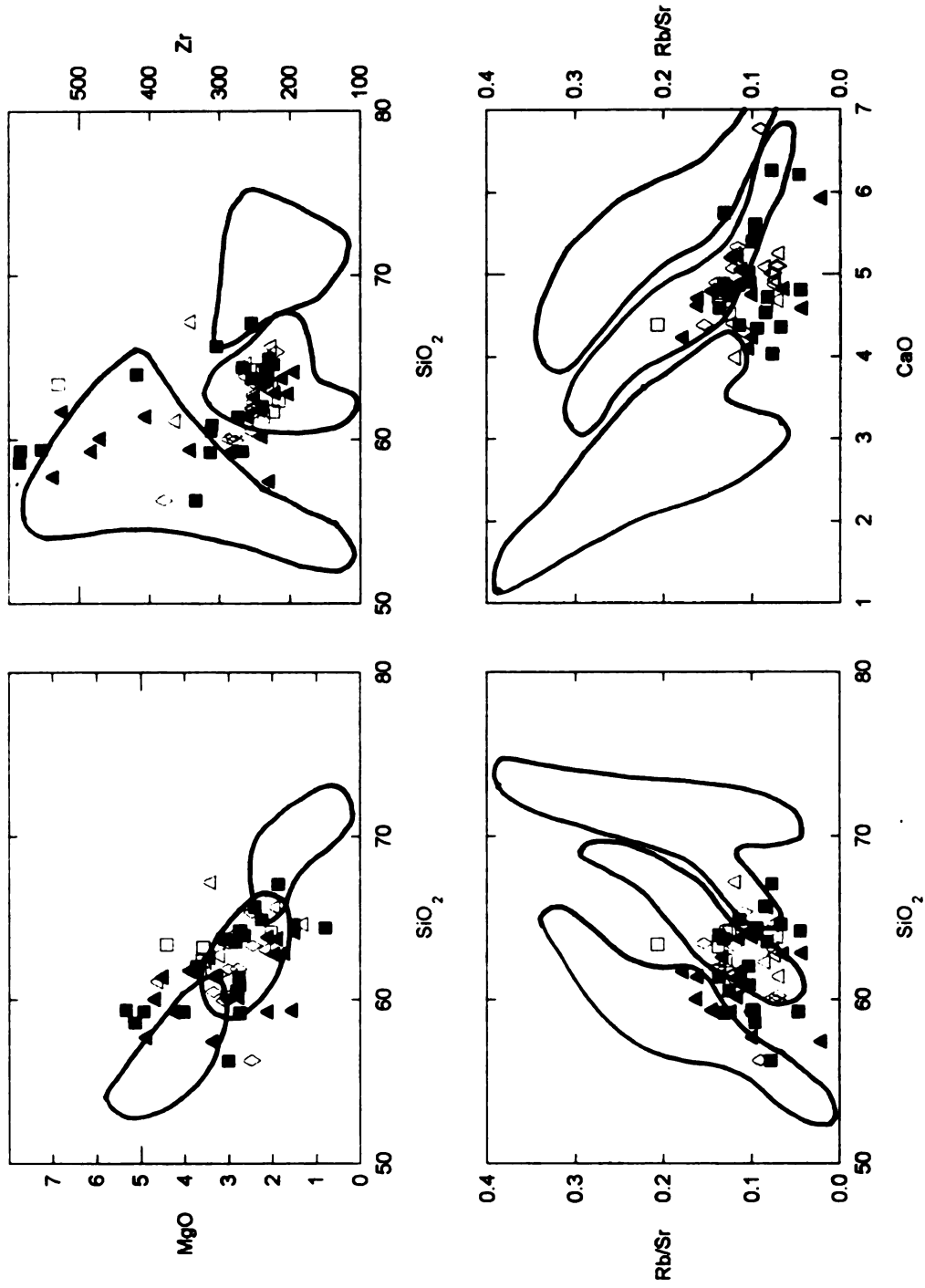
Figure 24. Comparison of the chemical compositions of the Western stocks (superimposed open areas) to the Keetley volcanics. Symbols for the Keetley volcanics are the same as in Figure 6.

implies that there is a minimum H_2O content and pressure that allows growth of

hornblende in the magma. The presence of very-fine grained pyroxenes nucleated around

reacted hornblendes as well as microphenocrysts of pyroxene in the matrix suggests that

hornblende became unstable while pyroxene became stable.

In general as the amount of H_2O in a silicate melt decreases the stability of hydrous

phases such as amphibole decreases (Eggler, 1972). An experimental study by Johnson

and Rutherford (1989) on the Fish Canyon Tuff indicates that at 2 kb hornblende becomes

unstable with less than .25 X_{H2O}. They found that for the Fish Canyon Tuff, in order for

amphibole to be stable at $P_{total} = 2$ kb X_{H2O} must be between .25 and .75. P, T and X_{H2O} can

be roughly estimated from hornblende instability. In calc-alkaline melts it appears that the

upper temperature stability limit of amphibole for any fugacity of H_2O in the fluid may

represent either incongruent melting of the amphibole or a reaction to clinopyroxene

(Eggler, 1972). Because of the calc-alkaline nature of the Keetley volcanics and the fact

that many of the samples contain hornblende phenocrysts rimmed by clinopyroxene, this

may represent a reaction controlled by the magma moving out of the stability field of

hornblende and into the stability field of pyroxene by a lowering of the P_{H2O} in the magma

as it ascended. The P, T and X_{H2O} conditions under which this process occurred may be

estimated to be between 930 °C and about 760 °C at 2 kb and below .25 X_{H2O} following

the experimental data of Johnson and Rutherford (1989).

Reverse Zoning in Plagioclase

The Keetley volcanics contain a significant population of reverse zoned

plagioclase phenocrysts. There are two possible explanations for this feature. One is that

an increase in pressure followed by a drop in pressure caused the rims of the plagioclase crystals to be more anorthitic than the inner parts of the crystal. This is caused by the fact that anorthite is more stable at elevated pressures than albite is. As a magma evolves under ideal conditions, one would expect to see the zoning of plagioclase become less anorthitic toward the rim. However, if there are cyclic increases and decreasses in pressure as one would expect to see in a volcanic system, increasing pressure results in more anorthitic rich composition of the plagioclase grains that are crystallizing (Figure 25). Another explanation for reverse zoning in plagioclase is magma mixing. The invasion of a more anorthitic magma into the magma chamber could also result in reverse zoning of plagioclase crystals. The variation from An_{30} to An_{53} of the rims of the plagioclase phenocrysts as well as the variation from An_{42} to An_{48} in the matrix plagioclase means that the not all of the plagioclase was in equilibrium with the same magma. The intrusion of a more mafic magma could have produced more anorthic rims on some of the plagioclase. Also, a more mafic magma could introduce other plagioclase grains with different rim compositions to the original magma. The fact that there is more than a bimodal distribution in anorthite compositions of the plagioclase rims implies that there is not a simple binary mixing cure. Instead there was probably more than one magmatic source involved. The anorthite variation within the rims and the matrix plagioclase could also be the result of changes in pressure as discussed above. It is difficult to distinguish between these two processes to explain the cause of reverse zoned plagioclase. The results of AFC modeling are consistent with magma mixing (see below) and therefore it is quite possible that the reverse zoning of the plagioclase is due to magma mixing.
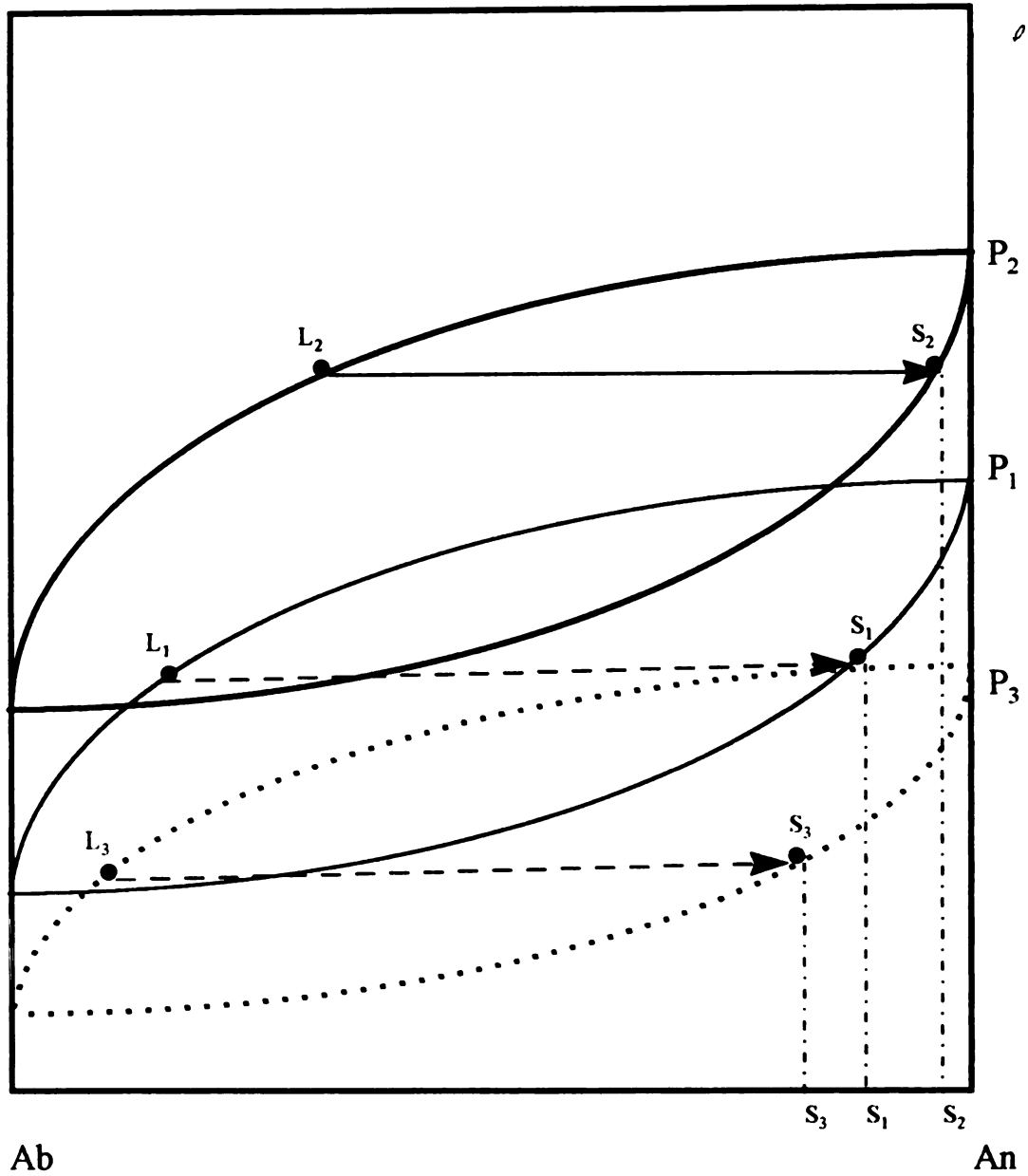
Figure 25. Theoretical plagioclase feldspar phase diagram illustrating the effects of varying pressure, where $P_2 > P_1 > P_3$.

Evaluation of Petrologic processes to Produce the Chemical Variation within the Keetley Volcanics; Fractional Crystallization, Magma Mixing, and Crustal Assimilation

Magma mixing, wall rock assimilation and fractional crystallization are all processes that can affect the chemical compositions of magmas. Tests of petrologic processes can be used to determine if the data set is consistent or inconsistent with a particular model but do not prove that a particular process is the cause of the chemical variation (Vogel, 1982). It is probable that more than one of these processes operates simultaneously resulting in complicated chemical trends to explain. Each of these processes are evaluated and are considered as possibilities for the chemical variation within the Keetley volcanics. Major and trace elements are used to evaluate these processes. Figure 26 shows the Keetley volcanics with two typical calc-alkaline differentiation trends of calc-alkaline rocks. The Keetley volcanics do not follow this typical trend and there is little coherence in the data array. Chemical compositions of the Keetley volcanics show significant scatter and can not be separated into different petrologic or chemical groups. Therefore it is very likely that more than one petrologic process has affected the Keetley volcanics. Whether or not magma mixing , assimilation or fractional crystallization or a combination of one or more of these processes have affected the evolution of the Keetley volcanics is a difficult question to answer directly because there is so little coherency in the data. However, these processes were evaluated and compared to other calc-alkaline suites of rocks.
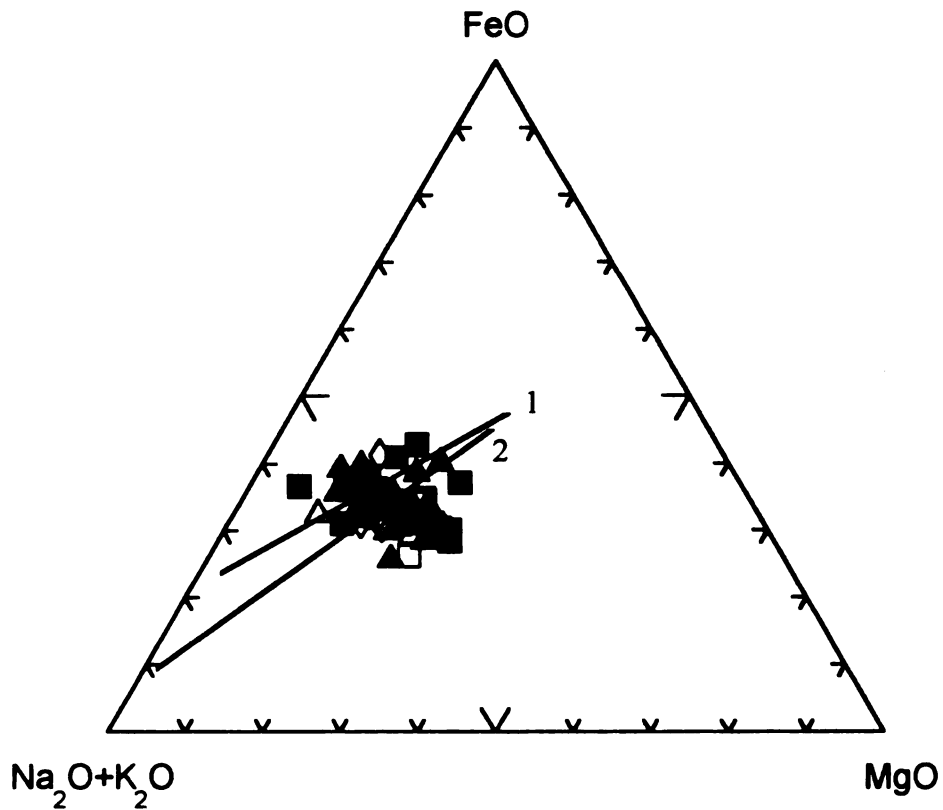
Figure 26. Typical differentiation trends of calc-alkaline rocks erupted within continental crust, 1 is for Lassen Peak, northern California and 2 is for Crater Lake National Park, Oregon (Hyndman, 1985 and references within). The Keetley volcanics clearly do not follow the typical calc-alkaline differentiation trend. Symbols for Keetley volcanics are the same as in Figure 6.

Fractional Crystallization

One mechanism for differentiation to produce andesites is by fractional

crystallization of a basalt parent, typically of plagioclase, orthopyroxene, amphibole and

magnetite (Gill, 1981). Statistical models of fractionation were tested and all were

unsuccessful, and cannot alone provide an explanation for the chemical variation within

the Keetley volcanics. Even smaller linear trends that occur within the entire data array

could not be modeled by fractionation. Clearly, linear trends within the total data set

obviously are not trends produced by crystal fractionation. There is also no petrographic

evidence of fractional crystallization, for example there are no accumulations of any

phenocrysts phases that seem to account for any variations in the chemistry such as

plagioclase accumulation, which would result in an overall increase in Sr.

The MELTS program (Ghiorso and Sack, 1995) was used to try to estimate

amounts and compositions of various fractionating phases over a temperature range of

1200°C to 900°C. The significant abundance of hornblende precludes the use of MELTS

program because it does not include hornblende as a fractionating phase in its calculations.

In a typical fractionated sequence of calc-alkaline andesites one would expect to

see near linear or curvilinear trends with little scatter within most major and trace element

chemical trends. Figure 27a-d illustrates the chemical composition of the Keetley

volcanics with recent analyses from calc-alkaline rocks of the Mogollon-Datil Volcanic

Field, New Mexico thought to be produced by fractionation (Davis and Hawkesworth,

1994). Notice the tight linear arrays for the Mogollon-Datil volcanics compared to the

large variation within the Keetley volcanics (Figure 27a-d). There must be more than one

Figure 27a-d. Comparison of a typical calc-alkaline fractionation trend (shaded areas) from the Mogollon-Datil volcanic field with the Keetley volcanics. Symbols for Keetley volcanics are the same as in Figure 6.
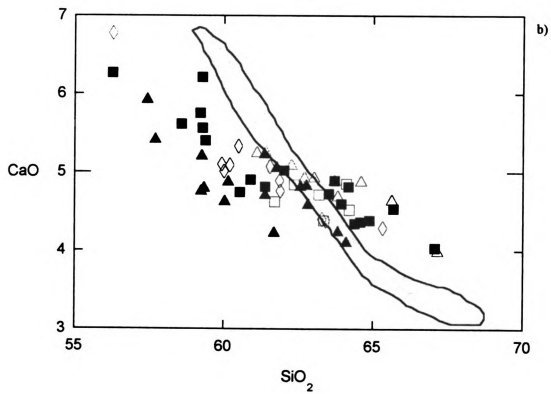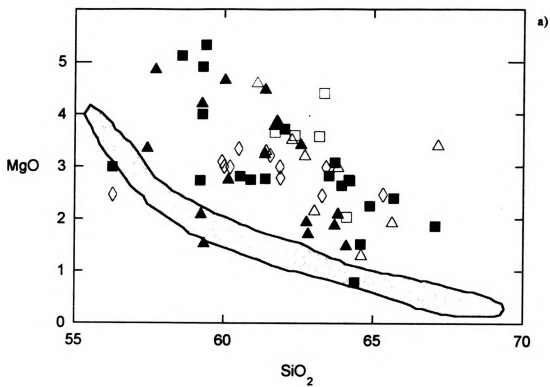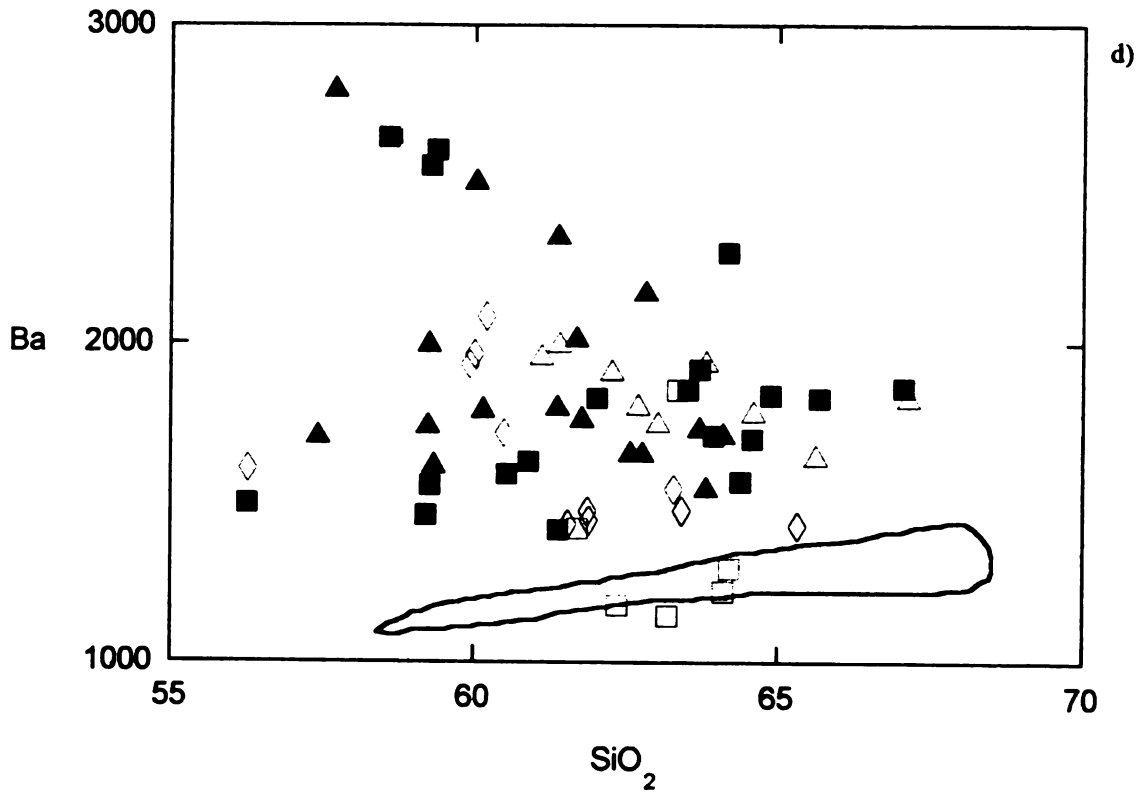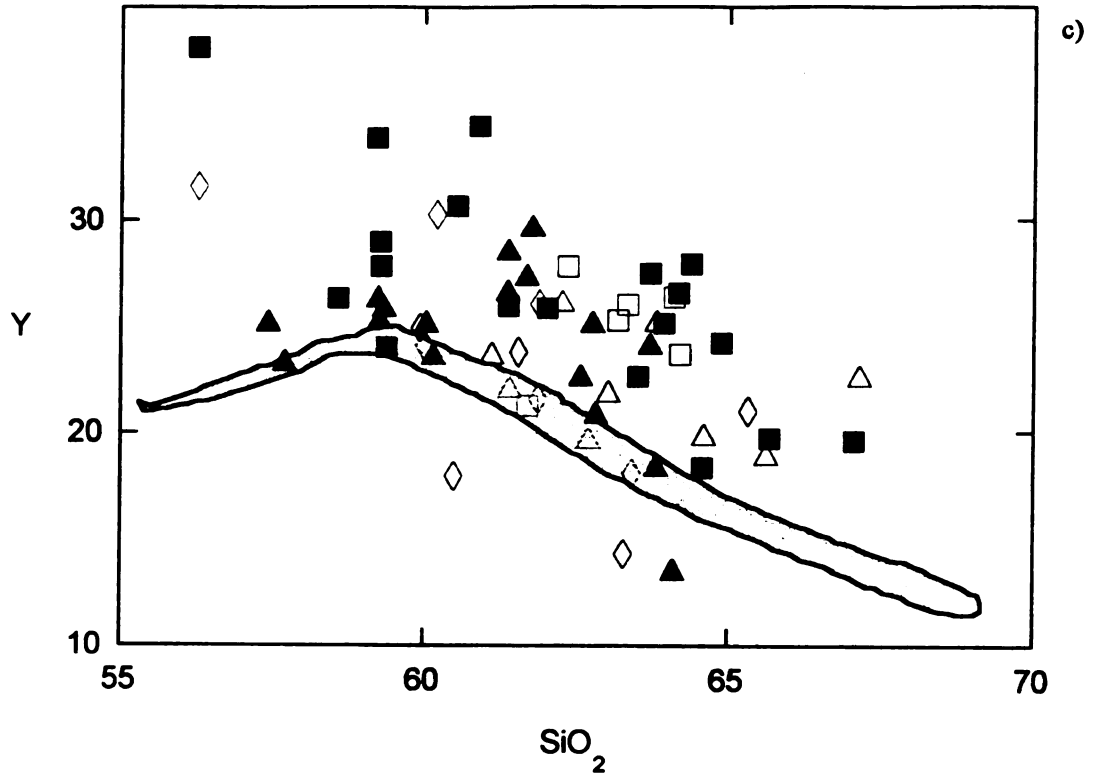
process affecting the petrogenesis of the Keetley volcanics, rather than simply one process such as fractional crystallization.

Magma Mixing

There are many documented cases of mixing a basalt with rhyolite or dacite to produce intermediate magmas such as andesites in several volcanic systems. Examples of this are the Coso volcanic field (Bacon and Metz, 1984), and the Medicine Lake Volcano (Grove et al., 1988). In both of these cases there is evidence of a hybrid magma including relict phenocrysts from both the mafic and felsic components (Bacon and Metz, 1984), as well as melted crustal xenoliths and reacted, resorbed and overgrown phenocrysts and xenocrysts (Grove et al., 1988). The Keetley volcanics show some evidence of mixing. Reacted and partially resorbed phenocrysts of hornblende are common but are believed to have resulted from lowering of pressure as the magma ascended, as discussed above. Mixing of basalt and silicic magma to produce an andesite, and eruption prior to re-equilibration of a hybrid magma can produce some of the same features, such as reacted phenocrysts, as does increasing P_{H2O} in a magma (Halsor and Rose, 1991). The Keetley volcanics also contain reverse zoned plagioclase phenocrysts which are probably the result of magma mixing.

Assimilation and Fractional Crystallization

All attempts at modeling magma mixing, or fractional crystallization as sole processes using multiple linear regression with the available end-members were unsuccessful. Magma mixing or fractional crystallization alone can not explain the chemical variation within the Keetley volcanics. However, combinations of crystal

fractionation and magma mixing within the available end members resulted in statistically

acceptable values. In these models acceptable results would include the sum of the

squares of the residuals being low, generally less than 1, the r^2 values being close to one

and the mixing coefficients being geologically reasonable, meaning that the mixing and

fractionating values have to be consistent with geologic and petrologic data (Vogel,

1982). In order to produce the intermediate, hybrid lava 17-31 IH a combination of

42.9% mafic end-member plus 65.1% silicic end-member with fractionation of 1.6%

hornblende, 3.7% plagioclase and 2.8% clinopyroxene from the mafic end-member result

in a sum of the squares of the residuals = .387. This combination of mixing and crystal

fractionation permits the AFC model as a possible explanation for the some of the

chemical variation within the Keetley volcanics. Similar results with the sum of the

squares of the residuals < 1 are reproducible using other silicic end-members (Table 11.).

However, this model does not prove that AFC alone caused the chemical variation.

Quartz and rare K-feldspar xenocrysts as well as possible xenoliths are found in

some of the samples, these may indicate assimilation of a silicic granitoid crust. It is not

possible to determine if the quartz and k-feldspar xenocrysts are the result of small pieces

of a granitoid contaminant being included or if they represent relict parts of large amounts

of incorporation of a granitoid that has been significantly melted (Lange and Carmichael,

1996). Therefore, even if there was contamination by a granitoid body through

assimilation, it is not possible to estimate the amount of assimilation of such a

contaminant. However, the rare occurrence and the resorbed, embayed texture of the

quartz grains suggest that they are xenocrysts. Whether or not what appear to be

xenoliths are actually xenoliths is difficult to determine because they have very similar

mineralogy to the Keetley volcanics, therefore they may just be aggregates of minerals from within the magma.

Origin of high-K calc-alkaline rocks and a Possible Petrogenetic Model for the Evolution of the Keetley Volcanics

There are two main tectonic settings in which high-K calc-alkaline rocks may be produced. One tectonic setting is a continental arc system and the other is a post collisional setting. The chemical and isotopic characteristics of magmas in an continental arc setting are believed to be the products of partial melting in the mantle wedge which is induced by incompatible element enriched fluids derived from a subducting slab. Subsequent to this the magmas rise to the continental crust and are further enriched in incompatible elements through assimilation (Roberts and Clemens, 1993). The amount of enrichment in incompatible elements from the crust is attributed to the thickness of the crust as well as the depth to the Benioff zone. The thicker the crust that the magma must pass through the more enriched in incompatibles it will become (Dickenson, 1975). Crustal contamination of the mantle derived parent magma will produce characteristic trace element and isotopic signatures, such as those examined in the classic continental arc setting of the Andes (Hildreth and Moorbath, 1988).

A second tectonic model for the origin of high-K calc-alkaline rocks is in post collisional settings (Pitcher, 1987 in Roberts and Clemens, 1993). Melting of the source rock occurs by interaction of mantle melts with the crust. Extension following thickening would then allow mantle upwelling and underplating of the lower crust by mantle derived mafic magmas (Sonder et al., 1987). The extra heat added to an already hot crust would

allow for partial melting to take place and these melts could then ascend through the crust (Sonder et al.; 1987, Dewey, 1984).

By Late Cretaceous time the western Cordillera had developed into an Andean type continental margin arc system, which produced mantle melts by the continuous subduction of the Farallon plate (Miller et al., 1992 and references therein). The relative rate of convergence between the Farallon plate and the North American plate increased between 75 and 70 Ma, continued from 65 to 55 Ma and began to decline between 55 and 40 Ma (Engebretson 1985). This slowing of convergence rate is attributed to a shallowing in subduction of the Farallon plate (Miller, 1992, and references therein).

The timing of compressional vs. extensional regimes in the Cordillera is related to the idea of migrating arc-magmatism (Coney and Reynolds, 1977). Migration of the magmatic arc in the southern Rocky Mountains is related to Late Cretaceous - Early Tertiary crustal shortening and simultaneous shallowing of the angle of subduction of the Farallon plate beneath North America (Coney and Reynolds, 1977). Constenius (1996) has recently reviewed the timing of the change from convergence to extension within the Cordillera. Based on ages of magmatism and basin formation, Constenius (1996) has suggested that during the Late Cretaceous to Early Eocene (72-54 Ma) accelerated subduction and/or shallowing of the subducting Farallon plate were occurring simultaneously with about 600 km of eastward progression of magmatism in the Cordillera. In the early-middle Eocene (53-51 Ma) there was a reduced rate of plate convergence, and steepening of the slab, resulting in westward migration and rollback. This caused widespread magmatism. In the middle Eocene (49-48 Ma) the onset of

normal faulting and basin-fill sedimentation in the Cordillera thrust belt was related to the westward movement of the Farallon plate from the Great Plains toward the Pacific coast. The normal faults superimposed half grabens on the deformed Cordillera thrust belt (Constenius, 1996).

The Uinta lineament was reactivated during the compressional stages of the Sevier and Laramide orogenies, which lasted from 145 Ma to 50 Ma overall. The onset of the change from compression to extension in the western U.S. began as a result of rollback of the Farallon plate (49-48 Ma), which in turn resulted in a thermal weakening of the crust (Constenius, 1996). The position of the subducted slab and the thermal state of the slab at 50, 35, 30, 20, 10 and 0 Ma were estimated by Severinghaus and Atwater (1990) based on magnetic anomalies, the time since subduction, and age of the slab upon entry into the trench. Based on these estimates Severinghaus and Atwater (1990) have concluded that by 35 Ma the subducted slab had been shortened along its entire length. This shortening or rollback of the slab is probably recorded by the westward sweep of magmatism in the western U.S. noted by Coney and Reynolds, (1977) and Cross and Pilger (1978). Cross and Pilger (1978) also suggest that the Farallon plate may have disassembled by breaking off into pieces during the rollback. The model proposed by Cross and Pilger (1978) of the rollback of the Farallon plate is illustrated in Figure 28. This figure illustrates the different stages of convergence of the North American plate and the Farallon plate and diagrams the break-up and roll-back of the subducted slab.

It is possible that the Wasatch intrusive belt and Keetley volcanics are a result of the steepening and rollback of the Farallon plate. The Uinta lineament was reactivated

Figure 28.   Stages of change in the angle of subduction of the Farallon plate and
              varying rates of convergence of the North American plate from 150 Ma to
              the present. Figure is modified from Cross and Pilger (1978).

SIERRA EPOCH
150-80 MYBP

LARAMIDE EPOCH
80-40 MYBP

40-30 MYBP

30-20 MYBP

BASIN RANGE
EPOCH
20-0 MYBP

PACIFIC | CAL | NV | UTAH | COLORADO |

0   500
KILOMETER
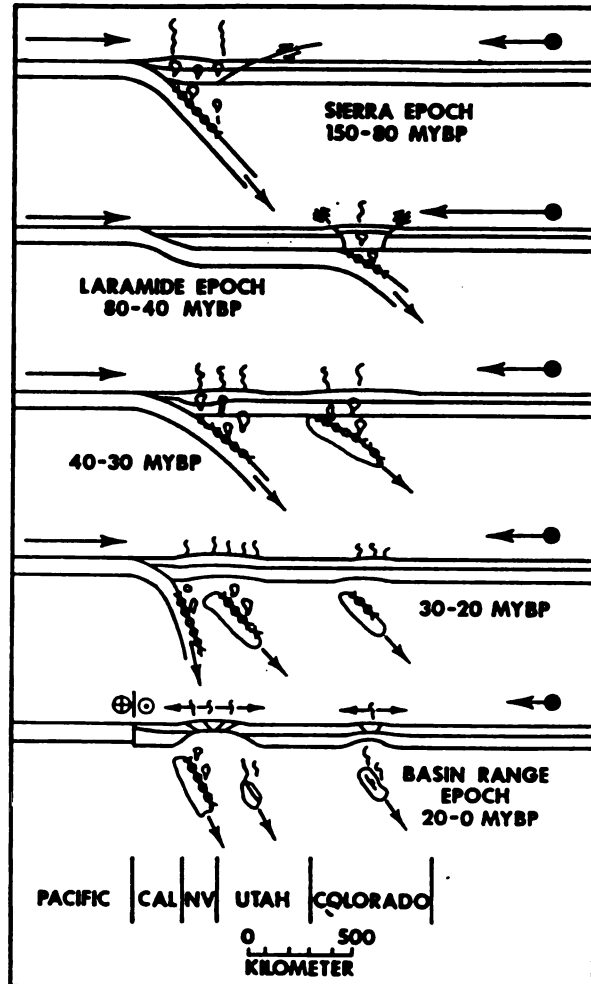
during the Sevier and Laramide orogenies. This linear weakness facilitated the emplacement of magmas related to the rollback of the Farallon plate to rise into the crust, beginning furthest east at 50 Ma and reaching Utah between 40 and 30 Ma. According to Severinghaus and Atwater (1990) at about 35 Ma the Farallon plate was steepening and rolling back underneath the western U.S., including north central Utah. Given the ages of the Wasatch intrusive belt and Keetley volcanics of around 34 Ma it is possible that the mantle derived magmas triggered by this process subsequently became buoyant and ascended into the Uinta lineament and formed the Wasatch intrusive belt.

Roberts and Clemens, (1993) evaluated a model for the origin and production of high-K calc-alkaline rocks such as the Keetley volcanics. They determined that partial melts from hydrated, meta-calc-alkaline and high-K calc-alkaline andesites and basaltic andesites are the most suitable source for producing high-K calc-alkaline rocks. The melts produced from these source rocks fall directly within the high-K calc-alkaline trend (Roberts, and Clemens, 1993, Beard and Lofgren, 1991). The presence of high-K calc-alkaline rocks therefore implies that there is a source of andesite at depth that is large enough to supply a melt. Partial melting of mafic to intermediate source compositions with H_2O contents between 0.7%and 1.6% have predicted volumes of generated melt between 30% and 60% at T= 900°C-950°C and P= 5-10 Kbar for fluid absent source rocks (Clemens, 1990; in Roberts and Clemens, 1993). The high volume of melt produced in these conditions precludes the need for fluids derived from elsewhere such as a subducting slab, to generate large enough volumes of melt that may move towards the surface (Roberts and Clemens, 1993).

A possible model for the evolution of the Keetley volcanics and Wasatch intrusive belt is that they were produced by partial melting of previously emplaced or underplated calc-alkaline rocks, which were related to subduction of the Farallon plate. These melts were subsequently emplaced along the Wasatch-Uinta lineament, which was a conduit along which these magmas could have been emplaced. A model of Cambray et al. (1993) may be applicable to the emplacement of the Wasatch intrusives. This model would invlove the development of releasing steps along larger normal faults within the Uinta lineament. These releasing steps could provide space for independent magmas to occur.

Conclusions

The purpose of this thesis was to determine the relationships between the Keetley volcanics and the Wasatch intrusive belt as well as to determine the cause of the chemical variation within the Keetley volcanics. The Keetley volcanics, the Alta stock and the eastern stocks have similar emplacement ages ranging from 33.5 - 34 Ma as well as similar chemical compositions. This suggests that these igneous bodies may have a genetic relationship.

The main conclusions from this thesis are the following. The Keetley volcanics have a significant variation in their chemical composition and this variation cannot be explained by fractional crystallization or magma mixing as separate processes acting independently. AFC models, however, permit magma mixing and crystal fractionation to produce an intermediate magma composition from mixing the most mafic and felsic end-members with simultaneous fractionation of amphibole, plagioclase and clinopyroxene from the mafic end-member. These models are reproducible using different end-members

from within the higher silica end with the most mafic end-member. The occurrence of reverse zoned plagioclase and quartz and K-feldspar xenocrysts are geologic evidence that some mixing/assimilation occurred.

The Keetley volcanics were most likely derived from partial melting of previously emplaced or underplated calc-alkaline rocks. The Uinta lineament is a weakness in the crust that was reactivated during the Laramide and Sevier orogenies. It is the conduit along which magma ascended to form the Wasatch intrusive belt and the Keetley volcanics. The rollback or break up of the Farallon plate is thought to have produced mantle melts which ascended to the crust causing melting of previously emplaced calc-alkaline rocks. The Uinta lineament acted as a conduit for the magmas to ascend further into the crust where the Wasatch intrusive belt and Keetley volcanics resulted. Upon ascent through the continental crust the magma underwent differentiation as well as assimilation and mixing resulting in a very diverse chemical composition for the Keetley volcanics.

APPENDICES

APPENDIX A

Appendix A. XRF detection limits for trace elements and statistics for major elelments analyzed from glass disks.

Element	Detection limit (ppm)	Major Oxide	TrMean (wt.%)	Std. Dev.
Ba	100	SiO_2	52.73	0.106
La	48	TiO_2	1.08	0.009
Cr	63	Al_2O_3	15.02	0.077
Ni	25	FeO	9.99	0.030
Zn	14	MnO	0.18	0.004
Rb	13	MgO	6.63	0.018
Sr	12	CaO	10.91	0.014
Y	14	Na_2O_3	2.18	0.018
Nb	15	K_2O	0.64	0.003
Zr	14	P_2O_5	0.14	0.005

APPENDIX B

Table 2. Whole rock XRF major oxide chemical anlayses.

Sample #	SiO2	TiO2	Al2O3	FeO	MnO	MgO	CaO	Na2O	K2O	P2O5
TK18-1	62.77	0.71	16.06	4.98	0.06	1.93	4.82	3.8	2.37	0.29
TK18-2	62.82	0.88	15.83	5.21	0.07	1.7	4.58	3.79	2.44	0.3
TK18-3	57.43	0.78	17.75	5.83	0.09	3.34	5.92	3.8	1.58	0.34
TK18-4	57.7	1.09	13.69	5.29	0.1	4.85	5.41	2.67	4.49	0.54
TK18-6	64.1	0.67	15.23	4.42	0.05	1.47	4.1	3.5	3.01	0.27
TK18-7	59.26	1.03	14.91	5.18	0.09	4.2	5.2	3.04	3.97	0.52
TK18-8	63.82	0.57	15.64	4.41	0.08	2.08	4.23	3.7	3.1	0.29
TK18-9	59.24	0.71	16.14	5.43	0.11	2.08	4.75	3.7	3.44	0.37
TK18-10	63.71	0.66	15.66	4.82	0.08	1.87	4.88	3.67	3.21	0.27
TK18-12	61.69	1.05	14.34	4.07	0.11	3.77	4.22	3.06	4.98	0.49
TK18-13A	59.34	0.81	16.39	5.64	0.07	1.52	4.79	3.78	3.47	0.42
TK18-13B	60.03	1.01	13.49	4.93	0.39	4.65	4.62	2.61	5.15	0.54
TK18-1	62.77	0.71	16.06	4.98	0.06	1.93	4.82	3.8	2.37	0.29
TK18-2	62.82	0.68	15.83	5.21	0.07	1.7	4.58	3.79	2.44	0.3
TK18-3	57.43	0.78	17.75	5.83	0.09	3.34	5.92	3.8	1.58	0.34
TK18-4	57.7	1.09	13.69	5.29	0.1	4.85	5.41	2.67	4.49	0.54
TK18-6	64.1	0.67	15.23	4.42	0.05	1.47	4.1	3.5	3.01	0.27
TK18-7	59.26	1.03	14.91	5.18	0.09	4.2	5.2	3.04	3.97	0.52
TK18-8	63.82	0.57	15.64	4.41	0.08	2.08	4.23	3.7	3.1	0.29
TK18-9	59.24	0.71	16.14	5.43	0.11	2.08	4.75	3.7	3.44	0.37
TK18-10	63.71	0.66	15.66	4.82	0.08	1.87	4.88	3.67	3.21	0.27
TK18-12	61.69	1.05	14.34	4.07	0.11	3.77	4.22	3.06	4.98	0.49
TK18-13A	59.34	0.81	16.39	5.64	0.07	1.52	4.79	3.78	3.47	0.42
TK18-13B	60.03	1.01	13.49	4.93	0.39	4.65	4.62	2.61	5.15	0.54
TK18-14	60.15	0.76	15.41	5.05	0.1	2.74	4.87	2.97	3.48	0.31
15-5I-80	61.11	0.86	15.17	5.06	0.1	4.59	5.24	3.37	3.52	0.44
15-9I-80	62.7	0.63	16.57	4.51	0.09	3.19	4.92	3.93	2.87	0.31
15-11I-80	67.15	0.77	13.29	4.03	0.07	3.39	3.98	3.07	3.27	0.4
15-14I-80	61.4	0.68	17.06	4.89	0.09	3.29	5.25	4.21	2.35	0.29

Table 2 (cont.)

15-15I-80	63.82	0.59	16.74	4.19	0.08	2.97	4.68	4.31	2.6	0.31
20-14I-80	82.27	0.67	16.3	4.82	0.09	3.5	5.08	3.92	2.63	0.34
20-17I-80	63.03	0.69	17.09	4.54	0.05	2.14	4.92	4.12	2.45	0.32
20-18I-80	65.63	0.6	15.7	3.9	0.05	1.92	4.63	3.82	2.58	0.29
20-19I-80	64.6	0.86	17.55	3.8	0.04	1.29	4.87	3.93	2.72	0.39
20-3FRAN	61.7	0.7	15.9	5.3	0.1	3.65	4.62	3.27	3.3	0.27
20-4FRAN	63.19	0.7	15.96	5.32	0.09	3.57	4.71	3.25	3.12	0.27
20-6FRAN	84.11	0.75	16.48	5.26	0.05	2.03	4.85	3.73	2.78	0.32
20-11FRAI	62.36	0.7	15.77	5.23	0.1	3.59	4.84	3.18	3.14	0.27
20-13FRAI	64.2	0.58	15.94	4.66	0.09	2.73	4.52	3.82	3.38	0.35
18-12PEO	63.35	1.03	14.45	4.46	0.12	4.4	4.38	3.19	4.99	0.54
18-14PEO	62.57	0.76	15.64	4.99	0.09	3.4	4.81	2.94	3.58	0.34
19-27PEO	61.37	0.85	16.19	6.03	0.1	3.23	5.22	3.19	3.2	0.38
19-28PEO	81.78	0.78	15.53	5.36	0.14	3.86	5.05	3.2	3.41	0.34
19-31PEO	61.38	0.93	14.4	4.76	0.12	4.47	4.7	2.99	4.55	0.48
17-28JD	61.39	0.89	16.41	5.25	0.11	2.76	4.81	3.93	3.85	0.43
18-8JD	56.27	0.86	18.11	6.9	0.14	2.99	6.26	3.64	2.6	0.52
18-9AJD	60.9	0.7	16.76	5.63	0.11	2.74	4.9	3.8	3.48	0.44
18-9BJD	80.55	0.89	16.68	5.5	0.11	2.81	4.74	3.61	3.71	0.4
19-1JD	63.94	0.87	14.55	4.83	0.07	2.63	4.59	3.34	4.22	0.54
19-2JD	59.28	0.73	18.5	5.51	0.11	4	6.21	3.87	1.46	0.34
19-3BJD	63.72	0.65	16.66	4.26	0.07	3.07	4.89	3.56	2.87	0.33
19-7JD	84.89	0.65	16.18	4.53	0.05	2.24	4.38	3.79	3.08	0.29
19-13JD	62.03	0.66	16.23	4.76	0.1	3.71	5.02	3.27	3.44	0.3
19-16JD	65.68	0.81	14.34	5.28	0.08	2.39	4.53	3.85	3.01	0.37
19-25JD	59.21	0.85	17.03	6.63	0.12	2.73	5.75	3.61	3.24	0.51
19-32JD	84.18	0.64	15.83	4.81	0.07	2.74	4.81	3.91	2.46	0.35
19-33JD	63.52	0.7	16.4	5.03	0.06	2.82	4.72	4.1	2.75	0.35
19-37JD	87.07	0.53	16.18	3.9	0.05	1.86	4.03	4.07	2.73	0.28
19-4JD	64.58	0.64	16.42	4.74	0.06	1.51	4.36	3.91	2.49	0.31
19-9JD	59.39	1.06	14.26	5.03	0.09	5.32	5.4	2.8	4.59	0.61

85

Table 2 (cont.)

19-10JD	59.29	1.06	14.1	5.4	0.08	4.91	5.56	2.98	4.46	0.63
19-11JD	58.59	1.06	14.17	5.3	0.08	5.12	5.61	2.74	4.43	0.63
19-17JD	64.39	0.74	16.63	4.46	0.02	0.79	4.34	3.77	3.16	0.51
16-04IH	65.32	0.63	15	4.62	0.06	2.46	4.29	3.71	3.22	0.39
16-09*IH	63.29	0.61	15.68	4.47	0.06	2.44	4.4	3.92	3.47	0.39
16-08IH	61.55	0.65	16.39	5.2	0.1	3.21	5.07	3.76	3.53	0.4
16-10IH	61.87	0.62	16.18	4.82	0.09	2.99	4.89	3.77	3.68	0.38
16-13IH	60.49	0.68	16.21	5.45	0.1	3.34	5.33	3.87	3.65	0.42
17-2IH	63.42	0.56	16.18	4.56	0.1	2.98	4.38	3.76	3.56	0.33
17-13IH	56.28	0.98	18.09	7	0.1	2.46	6.77	4.09	3.42	0.73
17-23IH	60.01	0.73	16.45	5.81	0.11	3	5.01	3.81	3.74	0.48
17-24IH	59.93	0.72	16.26	5.63	0.11	3.09	5.1	3.86	3.7	0.47
17-25IH	60.2	0.7	16.25	5.55	0.11	2.99	5.09	3.89	3.71	0.47
17-31IH	61.89	0.66	16.31	5.22	0.1	2.78	4.76	3.74	3.68	0.41

Table 3. Whole rock XRF trace element chemical analyses.

Sample #	Cr	Ni	Cu	Zn	Rb	Sr	Y	Zr	Nb	La	Ba
TK18-1	60.51	0.94	5.62	73.84	53.48	853.87	25.05	200.77	5	62.06	1651.92
TK18-2	64.46	1.38	7.28	52.28	47.24	1135	20.8	219.65	5	82.8	2156.62
TK18-3	76.01	2.43	8.28	90.87	19.75	985.35	25.09	228.08	2	35.96	1705.29
TK18-4	109.04	42.44	21.07	83.58	134.31	1376.16	23.22	535.55	5	109.74	2793.9
TK18-6	90.84	4.43	2.61	58.37	77.38	750.15	13.43	191.86	1	30.36	1710.69
TK18-7	125.24	30.2	14.69	79.55	124.22	1019.9	25.21	480.85	10	54.27	1995.35
TK18-8	67.15	1.38	0	67.21	88.33	899.85	18.33	228.7	4	118.38	1542.5
TK18-9	63.86	16.6	5.71	80.23	95.23	965.29	26.25	281.87	8	90.43	1739.21
TK18-10	88.5	7.45	0	50.2	87.06	773.65	24.03	209.51	10	89.37	1730.21
TK18-12	123.16	24.25	0	75.44	145.27	821.43	27.27	522.52	11	80.32	2012.74
TK18-13A	59.76	0	9.93	87.06	110.68	772.63	25.8	340.35	7	68.5	1614.06
TK18-13B	213.53	67.58	13.27	90.29	141.07	877.12	25.07	468.21	12	76.44	2505.3
TK18-1	60.51	0.94	5.62	73.84	53.48	853.87	25.05	200.77	5	62.06	1651.92
TK18-2	64.46	1.38	7.28	52.28	47.24	1135	20.8	219.65	5	82.8	2156.62
TK18-3	76.01	2.43	8.28	90.87	19.75	985.35	25.09	228.08	2	35.96	1705.29
TK18-4	109.04	42.44	21.07	83.58	134.31	1376.16	23.22	535.55	5	109.74	2793.9
TK18-6	90.84	4.43	2.61	58.37	77.38	750.15	13.43	191.86	1	30.36	1710.69
TK18-7	125.24	30.2	14.69	79.55	124.22	1019.9	25.21	480.85	10	54.27	1995.35
TK18-8	67.15	1.38	0	67.21	88.33	899.85	18.33	228.7	4	118.38	1542.5
TK18-9	63.86	16.6	5.71	80.23	95.23	965.29	26.25	281.87	8	90.43	1739.21
TK18-10	88.5	7.45	0	50.2	87.06	773.65	24.03	209.51	10	89.37	1730.21
TK18-12	123.16	24.25	0	75.44	145.27	821.43	27.27	522.52	11	80.32	2012.74
TK18-13A	59.76	0	9.93	87.06	110.68	772.63	25.8	340.35	7	68.5	1614.06
TK18-13B	213.53	67.58	13.27	90.29	141.07	877.12	25.07	468.21	12	76.44	2505.3
TK18-14	80.69	45.83	8.13	89.35	93.53	813.45	23.55	237.94	12	75.44	1789.56
15-5I-80	111.12	38.11	5.16	76.38	114.47	977.7	23.58	362.08	2.64	76.88	1954.96
15-9I-80	33.54	3.16	5.26	75.36	89.69	965.89	19.61	251.09	0	60.2	1798.98
15-11I-80	90.37	22.88	10.97	54.63	94.33	802.83	22.51	340.11	7.85	79.32	1823.12
15-14I-80	31.04	1.89	7.94	76.26	57.74	848.84	22	234.27	0	43.77	1993.94

Table 3 (cont.)

15-15I-80	48.21	22.66	0.95	64.04	68.65	989.87	25.12	261.73	2.75	64.82	1936.59
20-14I-80	59.65	5.18	11.41	75.6	78.49	936.9	26.05	251.59	4.32	60.21	1907.44
20-17I-80	32.05	3.96	9.36	67.93	65.9	897.54	21.79	228.29	6.82	44.42	1744.17
20-18I-80	27.8	0	18.9	55.46	68.42	842.88	18.84	225.1	5.95	70.52	1641.03
20-19I-80	72.03	0	17.81	72.41	70.56	959.01	19.77	261.25	3.23	61.7	1779.4
20-3FRAN	519.99	32.71	20.72	79.89	93.52	686.04	21.25	223.25	0.67	59.81	1419.09
20-4FRAN	29.7	0.55	20.2	77.09	89.98	655.15	25.27	225.35	3.96	65.46	1145.58
20-6FRAN	24.5	0	35.1	80.3	90.31	700.26	26.37	239.08	4.02	60.04	1222.95
20-11FRAI	26.19	0	10.9	77.59	85.71	664.72	27.83	215.94	3.16	59.79	1179.77
20-13FRAI	6.63	0	38.34	77.52	96.95	777.38	23.66	249.04	6.66	82.36	1294.57
18-12PEO	82.68	42.6	30.08	75.13	162.82	789.45	26.02	529.13	13.52	66.63	1853.84
18-14PEO	43.44	1.52	18.71	83.75	100	762.59	22.55	248.74	6.59	80.5	1652.89
19-27PEO	44.16	14.55	15.93	113.19	90.76	793.6	26.53	257.95	4.29	76.9	1796.83
19-28PEO	56.7	333.83	18.18	76.03	85.71	776.74	29.57	240.52	1.33	91.73	1760.54
19-31PEO	110.82	34.36	21.43	86.59	134.32	841.04	28.46	403.31	7.84	102.4	2334.75
17-28JD	9.95	0	15.58	76.62	122	895.6	25.95	273.41	1.34	80.85	1413.7
18-8JD	11.11	0	20.39	100.52	73.39	951.82	38.08	333.15	0.25	107.94	1496.52
18-9AJD	7.11	0	16.77	76.3	102.32	1007.21	34.4	309.81	3.07	104.76	1627.61
18-9BJD	19.07	0	18.68	78.97	111.68	896.66	30.63	311.15	0.29	125.19	1588.94
19-1JD	103.13	32.65	13.19	46.54	125.22	920.29	25.14	416.75	3.85	93.67	1711.28
19-2JD	28.64	12.07	23.56	90.02	45.49	987.2	28.97	266.02	0	74.74	1554.78
19-3BJD	58.2	101.34	18.5	72.62	110.65	845.62	27.47	253.36	0	93.49	1918.48
19-7JD	32.6	2.71	17.71	84.66	88.97	785.52	24.21	229.53	0	96.75	1837.31
19-13JD	48	11.41	10.04	76.26	92.33	902.79	25.83	238.58	0	55.51	1828.97
19-16JD	311.51	19.54	32.4	53.39	78.32	933.66	19.71	303.87	0	74.76	1827.86
19-25JD	4.74	0	13.28	99.49	111.35	856.01	33.87	312.28	3.08	98.46	1460.42
19-32JD	17	0	17.65	61.14	48.77	1099.37	26.56	233.96	0	121.26	2285.06
19-33JD	24.95	5.43	18.62	71.39	69.93	856.44	22.63	235.55	0	69.24	1854.29
19-37JD	7.27	2.04	9.16	47.01	70.98	930.91	19.59	253.65	0	55.81	1862.18
19-4JD	22.84	0	29.46	65.39	54.81	827.44	18.35	222.48	0	60.42	1700.62
19-9JD	71.64	27.28	28.79	85.88	138.09	1402.27	24.02	552.95	0.89	117.94	2606.65

88

Table 3 (cont.)

19-10JD	75.27	44.21	42.86	73.79	138.35	1440.5	27.83	582.32	0	138.45	2558.03
19-11JD	89.89	37	21.8	77.81	140.43	1473.45	26.29	584.16	0	112.77	2647.01
19-17JD	20.97	0	19.97	71.35	87.14	932.68	27.91	267.2	3.47	64.79	1565.48
16-04IH	36.67	2.56	25.35	70.71	89.66	830.34	21.01	219.72	4.86	82.5	1429.46
16-09*IH	23.16	0	18.37	57.44	101.23	846.31	14.32	236.81	4.52	55.73	1543.78
16-08IH	31.45	0	27.29	68.51	107.22	894.33	23.8	253.62	6.37	56.02	1433.11
16-10IH	19.02	5.93	14.71	63.79	121.83	877.66	21.59	250.21	2.34	53.59	1473.8
16-13IH	435.53	31.52	26.78	72.83	117.01	1014.49	17.97	252.66	0	77.23	1720.1
17-2IH	7.32	0	14.64	67.85	127.41	830.36	18.09	251.39	8.55	60.11	1475.79
17-13IH	10.14	4.72	29.22	98.7	104.14	1164.82	31.58	378.49	5.86	86.06	1606.83
17-23IH	0	0	20.88	83.16	108.18	1426.1	24.09	284.79	0	133.53	1967.73
17-24IH	0	10.04	17.2	83.45	100.08	1410.38	24.92	277.5	0	153.54	1934.55
17-25IH	6.58	0	20.89	81.82	98.41	1401.05	30.26	279.88	0	160.18	2085.26
17-31IH	2.02	0	12.37	80.07	112.57	881.63	26.03	252.73	5.01	72.29	1444.82

BIBLIOGRAPHY

Bibliography

Allmendinger, R.W., 1992. Fold and thrust tectonics of the western United States exclusive of the accreted terranes: The Geology of North America, v. G-3, The Cordilleran Orogen: Conterminous U.S. The Geological Society of America, p. 583-607.

Anderson, D.J., Lindsley, D.H., and Davidson, R.M., 1993. QUILF a Pascal program to assess equilibria among Fe-Mg-Mn-Ti oxides, pyroxenes, olivine, and quartz. Computers and Geosciences, v. 19; 9 p. 1333-1350.

Armstrong, R.L., 1968. Sevier orogenic belt in Nevada and Utah. Geological Society of America Bulletin, v. 79, p.429-458.

Bacon, C.R., and Metz, J., 1984. Magmatic inclusions in rhyolites, contaminated basalts, and compositional zonation beneath the Coso volcanic field, California. Contributions to Mineralogy and Petrology, v. 85, p. 346-365.

Beard, J.S., and Lofgren, G.E., 1991. Dehydration melting and water-saturated melting of basaltic and andesitic greenstones and amphibolites at 1, 3, and 6.9 kb. Journal of Petrology, v. 32, p. 365-401.

Boutwell, J.M, 1912. Geology and Ore Deposits of the Park City District, Utah. USGS Professional Paper 77, p.231.

Bromfield, M.D., Erickson, A.J., Jr., Haddadin, M.A., and Mehnert, H.H., 1977. Potassium-argon ages of intrusion, extrusion and associated ore deposits, Park City mining district, Utah. Economic Geology, v. 72, p. 837-848.

Bryan, W.B., Finger, L.W., and Chayes, F., 1969. Estimating proportions in petrographic mixing equations by least-squares approximation. Science, v. 163, p. 926-927.

Bryant, B. and Nichols, D.J., 1988. Late Mesozoic and early Tertiary reactivation of an ancient crustal boundary along the Uinta trend and its interaction with the Sevier orogenic belt. Geological Society of America, Memoir 171; Interaction of the Rocky Mountain Foreland and the Cordilleran Thrust Belt, p.411-430.

Calkins, F.C. and Butler, B.S., 1943. Geology and Ore Deposits of the Cottonwood-American Fork area, Utah. USGS Professional Paper 201, p. 1-145.

Cambray, F. William, and Holst, T.B., 1993. Kinematics of emplacement of the tertiary Alta Pluton, Central Wasatch Mountains, Utah. Transactions of American Geophysical Union (EOS), v. 74, p.578.

Carr, M.J., 1994. Igpet for Windows, Terra Softa Inc., Somerset, N.J., USA.

Constenius, Kurt, 1996. Late Paleogene extensional collapse of the Cordilleran foreland fold and thrust belt. Geological Society of America Bulletin, v.108, no. 1, p. 20-39.

Clemens, J.D., 1990. The granulite-granite connexion, in Vielzeuf, D., and Vidal, Ph., eds., Granulites and crustal evolution: Dordrecht, Netherlands, Kluwer, p. 25-36. In Roberts, M.P., and Clemens, J.D., 1993. Origin of high-potassium, calc-alkaline, I-type granitoids. Geology, v.21, p. 825-828.

Coney, P.J., and Reynolds, S.J., 1977. Cordilleran Benioff zones. Nature, v. 270, p. 403-406.

Crittenden, M.D., Jr., Stuckless, J.S., Kistler, R.W., and Stern, T.W., 1973. Radiometric dating of intrusive rocks in the Cottonwood area, Utah. U.S. Geological Survey Journal of Research, v. 1, p. 173-178.

Crittenden, M.D., 1977. Stratigraphic and Structural Setting of the Cottonwood Area, Utah: Symposium on Geology of the Cordilleran Hingeline; Rocky Mountain Association of Geologists, p. 363-379.

Cross, T.A., and Pilger, R.H. Jr., 1978. Constraints on absolute motion and plate interaction inferred from Cenozoic igneous activity in the western United States. American Journal of Science, v. 278, p. 865-902.

Davis, J., and Hawkesworth, C.J., 1994. Early calc-alkaline magmatism in the Mogollon-Datil Volcanic Field, New Mexico, USA. Journal of the Geological Society, London, v. 151, p. 825-843.

Dewey, J.F., 1984. Extensional collapse of orogens. Tectonics, v. 1, p. 1123-1139.

Dickenson, W.R., 1975. Potash-depth (K-h) relations in continental margins and intra-oceanic magmatic arcs. Geology, v. 3, p. 53-56.

Eardley, A.J., 1939. Structure of the Wasatch-Great Basin region. Geological Society of America Bulletin, v. 50, no. 8, p. 1277-1310.

Eggler, D.H., 1972. Amphibole stability in H_2O-undersaturated calc-alkaline melts. Earth and Planetary Science Letters, v. 15, p. 28-34.

Engebretson, D.C., Cox, A., Gordon, R.G., 1985. Relative motions between oceanic and continental plates in the pacific basin. Geological Society of America Special Paper, no. 206, 59p.

Feher, L.A., Constenius, K. N., and Vogel, T.A., 1996. Relationships between the Wasatch Intrusive Belt and the Keetley Volcanics, north-central, Utah. Geological Society of America Annual Meeting, Abstracts with Programs, v. 28, no. 7, p. 483.

Ghiorso, M.S. and Sack, R.O., 1995. Chemical mass transfer in magmatic processes. IV. A revised and internally consistent thermodynamic model for the interpolation and extrapolation of liquid-solid equilibria in magmatic systemas at elevated temperatures and pressures. Contributions to Mineralogy and Petrology, v.119, p. 197-212.

Gill, J.B., 1981. Orogenic andesites and plate tectonics. Springer, Berlin.

Grove, T.L., Kinzler, R.J., Baker, M.J., Donnely-Nolan, J.M., Lesher, C.E., 1988. Assimilation of granite by basaltic magma at Burnt Lava flow, Medicine Lake volcano, northern California: decoupling of heat and mass transfer. Contributions to Mineralogy and Petrology, v. 99, p. 320-343.

Halsor, S.P. and Rose, W.I., 1991. Mineralogical relations and magma mixing in calc-alkaline andesites from Lake Atitlan, Guatemala. Mineralogy and Petrology, v. 45, p. 47-67.

Hammerstrom, J.M., and Zen, E-an, 1986. Aluminum in hornblende: and empirical igneous geobarometer. American Mineralogist, v. 71, p. 1297-1313.

Hess, P.C., 1989. Origins of Igneous Rocks. Harvard University Press, Cambridge, Massachusetts, p. 149.

Hildreth, W., and Moorbath, S., 1988. Crustal contributions to arc magmatism in the Andes of central Chile. Contributions to Mineralogy and Petrology, v. 25, p. 894-928.

Hollister, L.S., and Grissom, G.C., Peters, E.K., Stowell, H.H., and Sisson, V.B., 1987. Confirmation of the empirical correlation of Al in hornblende with pressure solidification of calc-alkaline plutons. American Mineralogist, v.72, p. 231-239.

Hutchinson, R.W., and Albers, J.P., 1992. Metallogenic evolution of the Cordilleran region of the western United States in The Cordilleran Orogen: Conterminous U.S. The Geological Society of America, v. G-3, p. 629-652.

Hyndman, D.W., 1985. Petrology of Igneous and Metamorphic Rocks, 2nd edition, McGraw Hill, Inc., New York, p.257.

John, D.A., 1989. Geologic setting, depths of emplacement, and regional distribution of fluid inclusions in intrusions of the central Wasatch Mountains, Utah. Economic Geology, v.84, p. 386-409.

Johnson, M.C., and Rutherford, M.J., 1989. Experimentally determined conditions in the Fish Canyon Tuff, Colorado, magma chamber. Journal of Petrology, v. 30, part 3, p. 711-737.

Lange, R.A., and Carmichael, Ian S.E., 1996. The Aurora volcanic field, California-Nevada: oxygen fugacity constraints on the development of andesitic magma. Contributions to Mineralogy and Petrology, v. 125, p. 167-185.

Leveinen, J.E., 1994. Petrology of the Keetley Volcanics in Summit and Wasatch Counties, north-central Utah. University of Minnesota; M.S. p. 1.

Lindsley, D.H., and Frost, B.R., 1992. Equilibria among Fe-Ti oxides, pyroxenes, olivine, and quartz: Part 1. Theory. American Mineralogist, v.77, p. 987-1003.

McBirney, A. R., 1993. Igneous Petrology, 2nd edition, Jones and Bartlett Publishers, Inc., p. 319.

Miller, D.M., Nilsen, T.H., and Bilodeau, W.L., 1992. Late Cretaceous to early Eocene geologic evolution of the U.S. Cordillera: The Geology of North America, v. G-3, The Cordilleran Orogen: Conterminous U.S. The Geological Society of America, p.205-255.

Pitcher, W.S., 1987. Granites and yet more granites forty years on. Geologische Rundschau, v. 76, p. 51-79. In Roberts, M.P., and Clemens, J.D., 1993. Origin of high-potassium, calc-alkaline, I-type granitoids. Geology, v. 21, p. 825-828.

Roberts, M.P., and Clemens, J.D., 1993. Origin of high-potassium, calc-alkaline, I-type granitoids. Geology, v. 21, p. 825-828.

Severinghaus, J., and Atwater, T., 1990. Cenozoic geometry and thermal state of the subduction slabs beneath western North America. Geological Society of America, in Wernicke, B.P., ed., Basin and Range extensional tectonics near the latitude of

Las Vegas, Nevada: Boulder, Colorado, Geological Society of America memoir 196, p. 1-22.

Sonder, L.J., England, P.C., Wernicke, B.P., and Christiansen, R.L., 1987. A physical model for Cenozoic extension of western North America, in Coward, M.P., et al., eds., Continental extension tectonics. Geological Society of London Special Publication 28, p. 187-201.

Vogel, T.A, 1982, Magma mixing in the acidic-basic complex of Ardnamurchan: implications on the evolution of shallow magma chambers. Contributions to Mineralogy and Petrology, v. 79, p. 411-423.

Wernicke, B., 1992. Cenozoic extensional tectonics of the U.S. Cordillera, The Geology of North America, v. G-3, The Cordilleran Orogen: Conterminous U.S. The Geological Society of America, p. 553-581.

Wilson, M., 1989. Igneous Petrogenesis: A global tectonic approach, Unwin Hyman Ltd., London. p. 10.

Woodfill, R.D., 1972. A geologic and petrographic investigation of a northern part of the Keetley volcanic field, Summit and Wasatch Counties, Utah: Purdue University Ph.D. p. 120.